Ganoderic acid A suppresses glycolytic metabolism and promotes apoptosis in A549 lung adenocarcinoma cells with concurrent ALDOA downregulation

LONG MU[1*], YANZHAO CHEN[2*], QI ZHANG[1], YULU TIAN[1], SHUQI DING[1], HAOWEN LUO[1] and JUN XIAO[1]

[1]State Key Laboratory of Bioactive Substances and Functions of Natural Medicines, Institute of Materia Medica, Chinese Academy of Medical Sciences and Peking Union Medical College, Beijing 100050, P.R. China; [2]Institute of Basic Research in Clinical Medicine, China Academy of Chinese Medical Sciences, Beijing 100700, P.R. China

Received September 2, 2026; Accepted October 22, 2026

DOI: 10.3892/ol.2026.15952

Abstract. Ganoderic acid A (GAA) is a bioactive triterpenoid with reported anticancer activity, yet its effects on tumor glycolytic metabolism remain incompletely understood. The present study investigated the effects of GAA on glycolysis and apoptosis in A549 lung adenocarcinoma (LUAD) cells and examined the potential involvement of fructose-bisphosphate aldolase A (ALDOA). Cell viability was assessed using a Cell Counting Kit-8 assay, apoptosis was evaluated by Annexin V/PI flow cytometry and glycolytic activity was measured using a Seahorse XF-96 Extracellular Flux Analyzer. Western blotting, biochemical assays and public LUAD transcriptomic analyses were also performed. GAA reduced cell viability and increased apoptosis, accompanied by increased cleaved caspase-3 levels, decreased total caspase-3 and Bcl-2 expression and increased Bax expression. GAA also markedly suppressed glycolytic metabolism, as indicated by reductions in extracellular acidification rate, glycolytic capacity and reserve, glucose consumption, lactate production and intracellular ATP levels. Analysis of LUAD transcriptomic datasets showed that ALDOA was upregulated in tumor tissues and was associated with poorer overall survival, higher glycolysis-associated pathway activity and lower apoptosis-associated pathway activity. In A549 cells, GAA decreased ALDOA protein expression and total cellular aldolase activity in a concentration-dependent manner. Molecular docking and molecular dynamics simulations further predicted a plausible GAA-ALDOA interaction, while cellular thermal shift assays provided cellular target-engagement evidence supporting the potential interaction between GAA and ALDOA. However, the causal contribution of ALDOA to the metabolic and apoptotic effects of GAA remains to be established. Collectively, the present findings identified GAA as a suppressor of glycolytic metabolism in A549 cells and suggested that ALDOA-associated metabolic regulation may represent a potential mechanism underlying its pro-apoptotic pharmacological effects.

Correspondence to: Dr Haowen Luo or Dr Jun Xiao, State Key Laboratory of Bioactive Substances and Functions of Natural Medicines, Institute of Materia Medica, Chinese Academy of Medical Sciences and Peking Union Medical College, 2 Nanwei Road, Xicheng, Beijing 100050, P.R. China
E-mail: luohaowen@imm.ac.cn
E-mail: xiaojun@imm.ac.cn

*Contributed equally

Abbreviations: ALDOA, aldolase A; AUC, area under the curve; CETSA, cellular thermal shift assay; DEGs, differentially expressed genes; ECAR, extracellular acidification rate; GAA, ganoderic acid A; GO, Gene Ontology; GSEA, Gene Set Enrichment Analysis; HPA, Human Protein Atlas; HRs, hazard ratios; KEGG, Kyoto Encyclopedia of Genes and Genomes; LDCT, low-dose computed tomography; LUAD, lung adenocarcinoma; MD, molecular dynamics; MSigDB, Molecular Signatures Database; NSCLC, non-small cell lung cancer; OCR, oxygen consumption rate; PDB, Protein Data Bank; PPI, protein-protein interaction; Rg, radius of gyration; RMSD, root mean square deviation; RMSF, root mean square fluctuation; ROC, receiver operating characteristic; RT, room temperature; STR, short tandem repeat; WGCNA, weighted gene co-expression network analysis

Key words: ganoderic acid A, aldolase A, lung adenocarcinoma, glycolysis, apoptosis, tumor metabolism

Introduction

Lung cancer remains one of the most frequently diagnosed malignancies worldwide and a leading cause of cancer-associated mortality, with ~2 million new cases and 1.76 million mortalities reported annually (1,2). Non-small cell lung cancer (NSCLC) accounts for ~85% of lung cancer cases, with lung adenocarcinoma (LUAD) representing its predominant histological subtype. A notable proportion of patients with LUAD are diagnosed at an advanced stage, which contributes to the high mortality associated with this disease. Globally, lung cancer ranks second in cancer incidence and remains a leading cause of cancer-associated mortality, accounting for ~18% of all cancer mortalities (3,4). In China, 4.57 million new cancer

cases were reported in 2020, including ~816,000 cases of lung cancer, with 715,000 associated mortalities (5,6).

Despite marked advances in early detection, molecular classification, targeted therapy, and immunotherapy, treatment outcomes for advanced LUAD remain unsatisfactory. LUAD development involves complex interactions among environmental exposure, genetic alterations, metabolic reprogramming and changes in the tumor microenvironment (7). Tobacco exposure remains an important modifiable risk factor, whereas radon, occupational carcinogens and air pollution also contribute notably to lung carcinogenesis (8-10). Low-dose CT screening has improved the early detection of lung cancer in high-risk populations, particularly adults aged 50-80 years with a smoking history of at least 20 pack-years who currently smoke or have quit within the past 15 years (11); however, a number of patients still present with locally advanced or metastatic disease, with acquired drug resistance and disease recurrence remaining key therapeutic challenges (12). Therefore, identifying pharmacologically actionable molecular pathways and developing effective therapeutic agents for LUAD remain important research priorities.

Natural products have long served as an important source of bioactive compounds for anticancer drug discovery. PC-SPES, a botanical formulation formerly used as an alternative therapy in patients with cancer, contained *Ganoderma lucidum* (*G. lucidum*), also known as Lingzhi or Reishi, as one of its eight herbal components (13). *G. lucidum* has traditionally been used in Asia and has attracted marked attention because of its reported immunomodulatory and antitumor properties (14-16). Despite PC-SPES having been withdrawn from the market in 2002 due to contamination with prescription drugs such as warfarin (17,18), this experience highlighted the importance of investigating chemically defined and standardized bioactive constituents from medicinal plants and fungi.

G. lucidum has been used in Traditional Chinese Medicine for more than two millennia and increasing pharmacological evidence has indicated that its triterpenoids and polysaccharides exert antitumor effects in numerous malignancies, including lung, breast, colorectal and liver cancers (19-21). Ganoderic acid A (GAA) is one of the major bioactive triterpenoids of *G. lucidum* and has been reported to exert antiproliferative, pro-apoptotic and immunomodulatory effects (16,22,23). Previous studies have reported that GAA inhibits cell viability, migration and invasion in A549 and cisplatin-resistant A549/DDP cells, enhances chemosensitivity and promotes apoptosis through regulation of autophagy-associated signaling and the circular RNA-filamin A/microRNA-486-3p/cytochrome P450 family 1 subfamily A member 1/X-ray repair cross-complementing protein 1 axis (24). Notably, emerging evidence has also suggested that GAA reduces glucose consumption in lung cancer cells and disrupts IL-1β binding to IL-1R1 (25,26). GAA has been shown to reduce glucose consumption in A549 and H1299 cells and to regulate glucose transporters such as glucose transporter (GLUT)-1 and GLUT3 (25). In addition, a study combining computational and experimental approaches has suggested that GAA interacts with IL-1R1 and disrupts the binding of IL-1β to IL-1R1 (26). These findings suggest that the antitumor activity of GAA may involve both metabolic and signaling alterations. Despite this, the molecular basis associating GAA-induced metabolic suppression with apoptosis in LUAD, remains incompletely understood.

Aldolase A (ALDOA) is a key glycolytic enzyme that catalyzes an important step in glucose metabolism and is also implicated in non-canonical signaling processes associated with tumor progression. Elevated ALDOA expression has been reported in lung cancer and is associated with tumor progression, metastasis and unfavorable clinical outcomes (27). Mechanistically, ALDOA has been shown to activate the EGFR/MAPK signaling pathway and increase cyclin D1 expression, thereby promoting cell proliferation and G_1/S transition (28). ALDOA overexpression can also enhance lactate production, suppress plant homeodomain activity, stabilize HIF-1α and increase matrix metallopeptidase 9 expression, thereby facilitating tumor invasion and metastasis (29). These observations indicate that ALDOA may function as an important link between glycolytic reprogramming and malignant tumor behavior. However, whether ALDOA is associated with the pharmacological effects of GAA in LUAD, particularly its effects on glycolytic metabolism and apoptosis, remains unclear.

The present study aimed to investigate the antitumor effects of GAA in LUAD cells with a particular emphasis on glycolytic metabolism and apoptosis. Functional metabolic assays were used to determine the effects of GAA on extracellular acidification rate, glucose consumption, lactate production, ATP levels and cellular aldolase activity. Integrated analyses of The Cancer Genome Atlas (TCGA) and Gene Expression Omnibus (GEO) datasets were further performed to characterize the expression, prognostic relevance, glycolysis- and apoptosis-associated features, co-expression networks and immune associations of ALDOA in LUAD. Molecular docking and molecular dynamics simulations were additionally used to explore a potential interaction between GAA and ALDOA, followed by experimental evaluation of ALDOA protein expression and aldolase activity. Unlike previous studies that have primarily reported the effects of GAA on lung cancer cell viability, chemosensitivity, glucose consumption and potential interactions with glucose transporters (24,25), the present study further investigated the potential association among GAA-induced glycolytic suppression, apoptosis and ALDOA-related metabolic regulation. It was hypothesized that GAA suppresses glycolytic metabolism and promotes apoptosis in A549 cells in association with ALDOA-related glycolytic regulation.

Materials and methods

Chemicals and reagents. GAA (chemical abstracts service no. 81907-62-2; purity ≥98%) was purchased from Shanghai Yuanye Bio-Technology Co., Ltd. GAA was dissolved in DMSO to prepare a 1 M stock solution and further diluted with culture medium to the indicated concentrations. The final DMSO concentration did not exceed 0.02% (v/v). The Cell Counting Kit-8 (CCK-8) Cell Viability Assay Kit was obtained from Abcam (Fig. 1A). The FITC Annexin V Apoptosis Detection Kit and PI Staining Kit were purchased from BD Pharmingen (BD Biosciences). RPMI-1640 medium was purchased from Gibco (Thermo Fisher Scientific, Inc.). The ALDOA antibody (cat. no. 11217-1-AP) was obtained

from Proteintech Group, Inc. Antibodies against GAPDH (cat. no. 2118S), Bcl-2 (cat. no. 2876S), cleaved caspase-3 (cat. no. 9661), caspase-3 (cat. no. 9665), Bax (cat. no. 2772S) and HRP-conjugated secondary antibodies were obtained from Cell Signaling Technology, Inc. The BCA Assay Kit and Western Lightning™ Plus-ECL Assay Kit were supplied by Thermo Fisher Scientific, Inc.

Cell culture. A549 cells were obtained from Hunan Fenghui Biotechnology Co., Ltd. which were originally obtained from American Type Culture Collection. Cell lines were determined to be free of *Mycoplasma* and were authenticated using the short tandem repeat method, demonstrating high genetic consistency. The cells were cultured in RPMI-1640 medium (Gibco; Thermo Fisher Scientific, Inc.), supplemented with 10% FBS (GeminiBio LLC) and maintained in a humidified incubator at 37˚C with 5% CO_2.

Cell viability assay. Cell viability was assessed using a CCK-8 assay. Briefly, A549 cells were plated in 96-well plates at a density of $1x10^4$ cells/well and allowed to adhere for 24 h before treatment. The cells were then treated with GAA at concentrations of 0, 12.5, 25, 50, 100 or 200 μM for 24 h at 37˚C. Following treatment, 20 μl CCK-8 solution was added to each well and the plates were incubated for 4 h. For the expanded concentration-response analysis used to determine the 24-h IC_{50}, A549 cells were additionally treated with GAA at 6.25, 12.5, 25, 50, 100, 200, 250 and 300 μM for 24 h at 37˚C. Absorbance at 450 nm was measured using a Cytation 5 microplate reader (BioTek; Agilent Technologies, Inc.)

Flow cytometry. Effects of GAA on the induction of apoptosis in A549 cells were determined using flow cytometry. Briefly, A549 cells ($2x10^5$ cells/well) were seeded into 6-well plates and allowed to adhere for 24 h before treatment with 0, 25, 50, 100 or 200 μM of GAA for 24 h at 37˚C. The cells were dissociated by trypsinization and washed with PBS. According to the manufacturer's protocol for the Annexin V-FITC/PI Apoptosis Detection Kit [cat. no. AP101; MultiSciences (Lianke) Biotech Co., Ltd.], the harvested cells were resuspended in 1X binding buffer to a final concentration of $1x10^6$ cells/ml. Subsequently, 5 μl Annexin V-FITC and 10 μl PI were added to each sample, followed by incubation for 5 min at room temperature (RT) in the dark. Samples were analyzed using a Beckman Coulter CytoFLEX LX flow cytometer (Beckman Coulter, Inc.). Cell populations were first gated to exclude debris, followed by selection of the main cell population for Annexin V-FITC/PI analysis. Annexin V-positive/PI-negative cells were defined as early apoptotic cells, whereas Annexin V-positive/PI-positive cells were defined as late apoptotic cells. Total apoptotic cells were calculated as the sum of early and late apoptotic populations. Data were analyzed using CytExpert (version 2.3; Beckman Coulter, Inc.).

Western blotting analysis. To evaluate protein expression, A549 cells were cultured in 6-well plates ($2x10^5$ cells/well) and allowed to adhere for 24 h. The cells were treated with or without GAA for 24 h at 37˚C. Following treatment, the cells were lysed with 100 μl ice-cold RIPA buffer (cat. no. R0020; Beijing Solarbio Science & Technology Co., Ltd.), supplemented with protease and phosphatase inhibitors, using ultrasonication. After centrifugation at 4˚C for 10 min at 15,900 x g, the protein concentration in the lysate was measured using a BCA assay kit according to the manufacturer's instructions (30). A total of 30 μg of protein was separated by 10% SDS-PAGE and transferred onto a PVDF membrane. The membrane was blocked with 5% skim milk in TBST (with Tween-20) for 1 h at RT, followed by overnight incubation with primary antibodies (1:1,000 dilution) in 5% skim milk at 4˚C in TBST (30). The membranes were washed at least three times for 10 min each in TBST, then incubated with HRP-conjugated goat anti-rabbit IgG (H+L) secondary antibody (cat. no. db10002; Hangzhou Diagbio Biotechnology Co., Ltd.) (1:2,000 dilution) for 1 h at RT. After three additional washes in TBST, protein bands were detected using an ECL substrate. Images were captured using the Minichemi™ 610 Chemical Imaging System (Beijing Sage Creation Science Co., Ltd.) and the relative optical density of the bands from three independent experiments was analyzed using ImageJ software (version 1.52; National Institutes of Health) (30).

Data mining of GEO and TCGA database. Transcriptomic data from the GSE10072 dataset (31) were obtained from the GEO database (https://www.ncbi.nlm.nih.gov/geo/) and RNA-sequencing (RNA-seq) expression data together with corresponding clinical information for LUAD were obtained from TCGA database (https://portal.gdc.cancer.gov/). The TCGA-LUAD cohort comprised 575 samples, including 516 primary tumor tissues and 59 normal lung tissues. Differential expression analysis between tumor and normal samples was performed using the 'edgeR' R package (32). Briefly, raw count data were organized into a DGEList object and normalized using the trimmed mean of M-values method. A design matrix was constructed according to sample group and biological dispersion was estimated using the 'edgeR' framework (33). Differential expression between LUAD and normal lung tissues was subsequently assessed using the quasi-likelihood negative binomial generalized log-linear model and quasi-likelihood F-test implemented in 'edgeR' (34). P-values were adjusted for multiple testing using the Benjamini-Hochberg method. Genes with an adjusted $P<0.05$ and $\log_2$ fold change (FC)>1 were considered to be differentially expressed. Volcano plots and heatmaps were generated using the 'ggplot2' (35) and 'pheatmap' (36) R packages, respectively. In addition, protein expression data from the Human Protein Atlas (HPA; http://www.proteinatlas.org/) were used to evaluate the protein-level expression of ALDOA in LUAD.

Survival analysis. Kaplan-Meier survival analysis was performed using R software (version 4.4.0; Posit Software, PBC) (37) was performed to evaluate the association between ALDOA expression and overall survival in the TCGA-LUAD cohort. Patients were divided into ALDOA-high (expression >8.3745; n=258) and ALDOA-low (expression ≤8.3745; n=258) groups according to the median ALDOA mRNA expression level (8.3745). Survival distributions between the two groups were compared using the log-rank test. $P<0.05$ was considered to indicate a statistically significant difference.

Gene Ontology (GO) and Kyoto Encyclopedia of Genes and Genomes (KEGG) enrichment analysis of the differentially expressed genes (DEGs). GO (https://geneontology.org/) and KEGG (https://www.genome.jp/kegg/) pathway enrichment analyses of the DEGs were performed using the 'clusterProfiler' (38) and 'enrichplot' (39) R packages in R software (version 4.4.0; Posit Software, PBC). P-values from the enrichment analyses were adjusted using the Benjamini-Hochberg method and terms with an adjusted $P<0.05$ were considered to be significantly enriched. Representative enrichment results were visualized using bubble plots and bar plots generated with the 'ggplot2' R package (35).

Gene Set Variation Analysis (GSVA)-based pathway activity analysis of clinical LUAD data. GSVA was performed to estimate pathway activity at the individual-sample level in the TCGA-LUAD cohort according to the method previously described by Hänzelmann *et al* (40). Gene sets were obtained from the Molecular Signatures Database (MSigDB; version 7.4), using the c2.cp.kegg.v7.4.symbols.gmt collection (41). Sample-specific enrichment scores were calculated to generate a pathway activity matrix for subsequent analyses. The KEGG apoptosis and glycolysis/gluconeogenesis gene sets were selected to evaluate apoptosis- and glycolysis-associated pathway activity, respectively. Pearson correlation analysis was performed to assess the association between ALDOA expression and the corresponding GSVA scores across LUAD samples (42). For glycolysis-related analysis, TCGA-LUAD samples were further divided into ALDOA-high (expression >8.3745; n=258) and ALDOA-low (expression ≤8.3745; n=258) groups according to the median ALDOA expression level (8.3745) and differences in glycolysis GSVA scores between the two groups were statistically evaluated. Given that these analyses focused on prespecified apoptosis- and glycolysis-related gene sets rather than pathway-wide screening, nominal P-values were reported for these comparisons.

Construction and topological analysis of the PPI network. A total of 87 apoptosis-related genes used in the present study were submitted to the Search Tool for the Retrieval of Interacting Genes/Proteins (STRING) database (version 12.0; https://cn.string-db.org/) to construct a PPI network for *Homo sapiens* (43). A minimum required interaction score of 0.9 was applied and disconnected nodes were excluded from network visualization. The resulting interaction network was imported into Cytoscape software (version 3.10) for visualization and topological analysis (44). Degree centrality was calculated for each node and the top 20 genes ranked by degree value were identified. In addition, the CytoNCA plugin was used to further evaluate network centrality and identify key hub proteins within the apoptosis-related PPI network (45).

Glucose consumption and lactate production and ATP measurement. A549 cells were treated with the indicated concentrations of GAA or vehicle control for 24 h at 37˚C. Following treatment, culture supernatants were collected for the measurement of glucose consumption and lactate production using the corresponding commercial assay kits (Glucose Assay Kit, cat. no. F006-1-1; Lactic Acid Assay Kit, cat. no. A019-2-1; both, Nanjing Jiancheng Bioengineering Institute) (46). All procedures were performed according to the manufacturers' instructions. Absorbance was measured at 530 nm using a Cytation 5 microplate reader (BioTek; Agilent Technologies, Inc.) and glucose and lactate concentrations were calculated from the respective standard curves. In parallel, treated cells were collected and lysed in 300 μl hot double-distilled water by ultrasonication, followed by incubation in a boiling water bath (100˚C) for 10 min, for the determination of intracellular ATP levels using a commercial ATP assay kit (cat. no. A095-1-1; Nanjing Jiancheng Bioengineering Institute) according to the manufacturer's protocol. ATP levels were calculated based on the corresponding standard curve. All measurements were performed in three independent experiments. The measured metabolic parameters were normalized to total cellular protein content.

Aldolase activity assay. Cellular aldolase activity was measured using an Aldolase Activity Assay Kit (cat. no. ab196994; Abcam) according to the manufacturer's instructions (47). Protein concentrations of the cell lysates were determined using a BCA assay and aldolase activity was normalized to total protein content.

Extracellular acidification (ECAR) measurements and oxygen consumption rate (OCR) measurements. Glycolytic activity was assessed by measuring the ECAR using a Seahorse XF-96 Extracellular Flux Analyzer (Agilent Technologies, Inc.) as previously described (46). A549 cells were seeded into XF-96 cell culture microplates at a density of 4,000 cells per well and allowed to adhere for 24 h. The cells were then treated with GAA at concentrations of 0, 25, 50, 100 or 200 μM for an additional 24 h at 37˚C in a humidified atmosphere containing 5% CO_2. Before ECAR measurement, the culture medium was replaced with Seahorse basal assay medium supplemented with 2 mM glutamine and the cells were equilibrated in a non-CO_2 incubator for 1 h. Basal ECAR was recorded, followed by sequential injection of glucose (10 mM), oligomycin (1 μM) and 2-deoxy-D-glucose (2-DG; 100 mM). Additional ECAR measurements were performed in cells treated with 0, 6.25 or 12.5 μM GAA. Under the same low-dose conditions, OCR was recorded at baseline and after sequential addition of oligomycin (1 μM), carbonyl cyanide-p-trifluoromethoxyphenylhydrazone (1 μM) and antimycin A (1 μM). Glycolysis, glycolytic capacity and glycolytic reserve were calculated from the ECAR profiles according to the manufacturer's instructions. ECAR and OCR values were normalized to total cellular protein content determined by BCA assay. All experiments were independently repeated three times.

Weighted gene co-expression network analysis (WGCNA) and Gene Set Enrichment Analysis (GSEA) analysis of clinical LUAD data. WGCNA was performed using the TCGA-LUAD transcriptomic dataset to identify gene co-expression modules and characterize the network context of ALDOA (48). The 'WGCNA' R package was used to construct a weighted co-expression network (49). An appropriate soft-thresholding power was selected according to the scale-free topology criterion and genes were subsequently clustered based on topological overlap. Co-expression modules were identified using hierarchical clustering combined with the dynamic tree cut

algorithm and were assigned different colors (50). Following module assignment, the module containing ALDOA was identified based on the gene-module membership results. Genes within the ALDOA-containing module were subjected to functional enrichment analysis to characterize their potential biological functions. GSEA was further performed to evaluate the association of this module with apoptosis-related signaling using the 'clusterProfiler' R package (38) and the enrichment results were visualized using the 'enrichplot' R package (39).

Identification and correlation analysis of immune infiltrating cells in LUAD. To estimate immune cell infiltration based on gene expression profiles, Cell-type Identification By Estimating Relative Subsets Of RNA Transcripts (CIBERSORT) was applied using the LM22 leukocyte signature matrix (51), with the 'preprocessCore' R package (37) used for data preprocessing. CIBERSORT was performed with 100 permutations and quantile normalization enabled. No additional filtering based on the CIBERSORT deconvolution P-value was applied. The sum of the estimated proportions of all immune cell types in each sample is equivalent to 1 (52). The relative proportions of the 22 immune cell populations in each sample were quantified using the expression data from the TCGA database. A box plot was used to visualize the distribution of immune cell populations between LUAD tumor and normal lung tissues. Differences in immune cell proportions between tumor and normal tissues were evaluated using the Wilcoxon rank-sum test and the resulting P-values were adjusted for multiple comparisons using the Benjamini-Hochberg false discovery rates (FDR) method. Pairwise associations among the 22 immune cell populations were assessed using Spearman correlation analysis, with Benjamini-Hochberg FDR correction applied to the corresponding multiple correlation tests. Associations between ALDOA expression and individual immune cell populations in LUAD tumor samples were also evaluated using Spearman correlation analysis and the resulting P-values were similarly adjusted using the Benjamini-Hochberg FDR method. An FDR-adjusted $P<0.05$ was considered to indicate a statistically significant difference.

Molecular docking. The three-dimensional crystal structure of human ALDOA was obtained from the Protein Data Bank (PDB; https://www.rcsb.org/; ID: 2ALD) (53). The three-dimensional structure of GAA (PubChem compound ID: 471002) was obtained from the PubChem database (https://pubchem.ncbi.nlm.nih.gov/). The protein structure was prepared by removing crystallographic water molecules and other non-essential heteroatoms, followed by the addition of hydrogen atoms using AutoDockTools (version 1.5.7) (54,55). The prepared receptor and ligand structures were subsequently converted into PDBQT format for molecular docking. For GAA-ALDOA docking, the grid box was centered at x=2.61, y=35.26 and z=47.04, with dimensions of 37.5x37.5 x 37.5 $Å^3$. Molecular docking was performed using AutoDock Vina (version 1.2.7) (56,57). The predicted GAA-ALDOA binding poses and ligand-residue interactions were visualized using the University of California, San Francisco ChimeraX (version 1.8; Resource for Biocomputing, Visualization, and Informatics) software.

Molecular dynamics simulation. All molecular dynamics simulations were performed using GROMACS (version 2025.3; https://www.gromacs.org/). The Chemistry at Harvard Macromolecular Mechanics (CHARMM) force field was employed for the protein-ligand system, with system parameters generated through the CHARMM graphical user interface web server. The transferable intermolecular potential with 3 points (TIP3P) water model was used to solvate the system. The GAA-ALDOA complex was placed in a cubic simulation box with dimensions of 8.6x8.6x8.6 nm^3. The system was solvated with 17,966 TIP3P water molecules and neutralized by adding 51 Na^+ and 53 Cl^- ions, corresponding to an ionic strength of ~150 mM. The final system contained 59,627 atoms. Following system preparation and equilibration, three independent 200-ns production molecular dynamics simulations were performed to evaluate the conformational stability of the predicted GAA-ALDOA complex. The resulting trajectories were analyzed using the built-in GROMACS tools. Root mean square deviation (RMSD) was calculated to assess the overall conformational stability of the complex, root mean square fluctuation (RMSF) was used to evaluate residue-level flexibility and radius of gyration (Rg) was calculated to assess the overall structural compactness of ALDOA. In addition, a two-dimensional free energy landscape was constructed using RMSD and Rg as collective variables to characterize the key conformational states sampled by the GAA-ALDOA complex during the simulations.

Cellular thermal shift assay (CETSA). A549 cells were treated with GAA (100 μM) or DMSO for 1 h at 37˚C, harvested and resuspended in PBS containing protease inhibitors. Cell suspensions were aliquoted and heated at 37, 42, 47, 52, 57 or 62˚C for 3 min, followed by cooling at 25˚C for 3 min. Cells were lysed by three freeze-thaw cycles in liquid nitrogen and the soluble fractions were collected after centrifugation. ALDOA abundance in the supernatants was subsequently determined by western blotting. The experiment was independently repeated three times.

Statistical analysis. Experimental data are presented as the mean ± SEM from independent experiments. Normality of glycolysis GSVA scores was assessed using the Shapiro-Wilk test. Unpaired Student's t-tests were used for comparisons of ALDOA expression and apoptosis-related gene expression scores between tumor and normal tissues, whereas the Mann-Whitney U test was used to compare glycolysis GSVA scores between ALDOA-high and ALDOA-low groups. A one-way ANOVA and Bonferroni post hoc correction were used for univariate multiple comparisons. A two-way ANOVA was used for multiple comparisons of two variables in CETSA experiments, followed by Bonferroni post hoc tests. The log-rank test was used for survival analysis, the Wilcoxon rank-sum test for immune infiltration comparisons and Pearson or Spearman correlation analysis for the corresponding correlation analyses. $P<0.05$ was considered to indicate a statistically significant difference. For bioinformatic analyses involving multiple testing, Benjamini-Hochberg-adjusted P-values or FDR values were used where specified in the corresponding Methods sections; otherwise, nominal P-values are explicitly indicated.

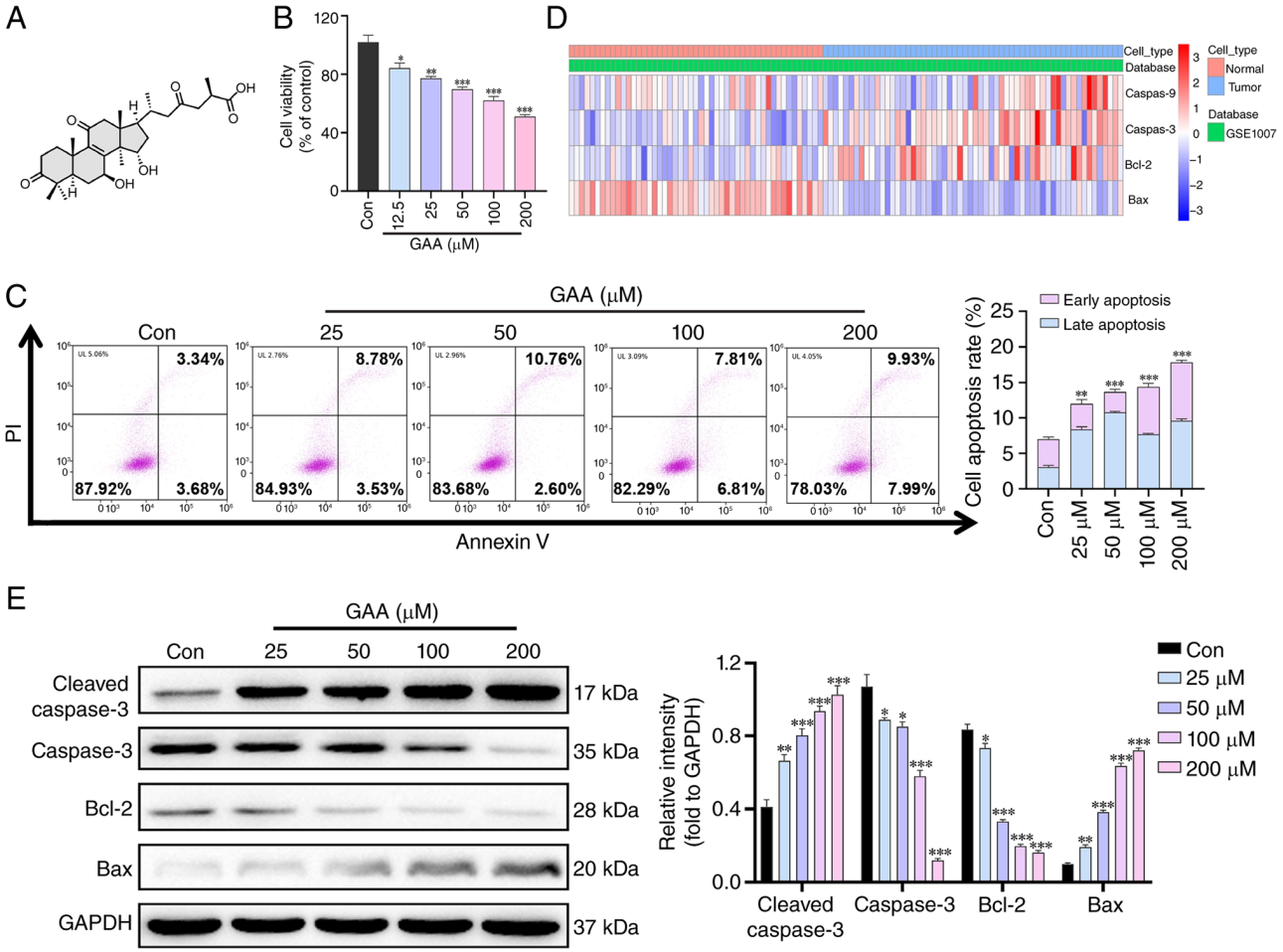


Figure 1. GAA induces apoptosis in a dose-dependent manner in A549 cells. (A) Chemical structure of GAA. (B) Cell viability of A549 cells was evaluated by Cell Counting Kit-8 assay after treatment with increasing concentrations of GAA (12.5-200 μM) for 24 h. (C) Apoptosis of A549 cells were analyzed by flow cytometry using Annexin V/PI staining after 24 h of GAA treatment. (D) Heatmap showing the expression patterns of apoptosis-related genes in lung of the normal patients and lung adenocarcinoma patients using the Gene Expression Omnibus database GSE10072. (E) Western blotting analysis of apoptosis-related proteins, including cleaved caspase-3, caspase-3, Bcl-2 and Bax, in A549 cells treated with GAA for 24 h. The relative intensities of proteins were normalized against GAPDH. Data are presented as mean ± SEM from three independent experiments. Statistical significance was assessed using one-way ANOVA followed by Bonferroni's multiple-comparison test. *P<0.05, **P<0.01 and ***P<0.001 vs. control. GAA, ganoderic acid A; Con, control.

GraphPad Prism (version 9; Dotmatics) was used for data plotting.

Results

GAA dose-dependently suppresses A549 cell viability and induces apoptosis. To evaluate the cytotoxic effects of GAA on lung adenocarcinoma cells, A549 cell viability was first assessed using a CCK-8 assay. As shown in Fig. 1B, treatment with increasing concentrations of GAA (12.5-200 μM) for 24 h resulted in a significant reduction in cell viability, demonstrating a clear dose-dependent cytotoxic effect. To determine whether the observed inhibition was associated with apoptosis, flow cytometric analysis was subsequently performed. GAA treatment (25-200 μM) increased the proportion of apoptotic cells in a concentration-dependent manner (Fig. 1C). Both early and late apoptotic populations contributed to the overall increase in apoptosis following GAA treatment. These findings indicate that the inhibitory effect of GAA on A549 cell viability is accompanied by increased apoptosis.

To further elucidate the molecular mechanisms underlying GAA-induced apoptosis, key regulators of the mitochondrial apoptotic pathway were examined. Members of the Bcl-2 family and caspase cascade serve central roles in apoptotic signaling (58). In addition, the anti-apoptotic protein Bcl-2 and the pro-apoptotic protein Bax are well-established modulators of programmed cell death (59,60). Using the publicly available GEO dataset (GSE10072), the present study first analyzed the expression patterns of apoptosis-associated genes in normal lung tissues and LUAD samples. As shown in Fig. 1D, precursor caspase-9, precursor caspase-3 and Bcl-2 were markedly upregulated in LUAD tissues, whereas Bax expression was markedly downregulated. Western blotting analysis further revealed that GAA treatment significantly increased the level of cleaved caspase-3 while significantly decreasing the expression of total caspase-3 and Bcl-2 in a dose-dependent manner. Meanwhile, Bax expression was significantly progressively elevated following GAA exposure (Fig. 1E). These results demonstrate that GAA activated the caspase-dependent apoptotic pathway and promoted a shift in the Bax/Bcl-2 balance toward a pro-apoptotic state in A549

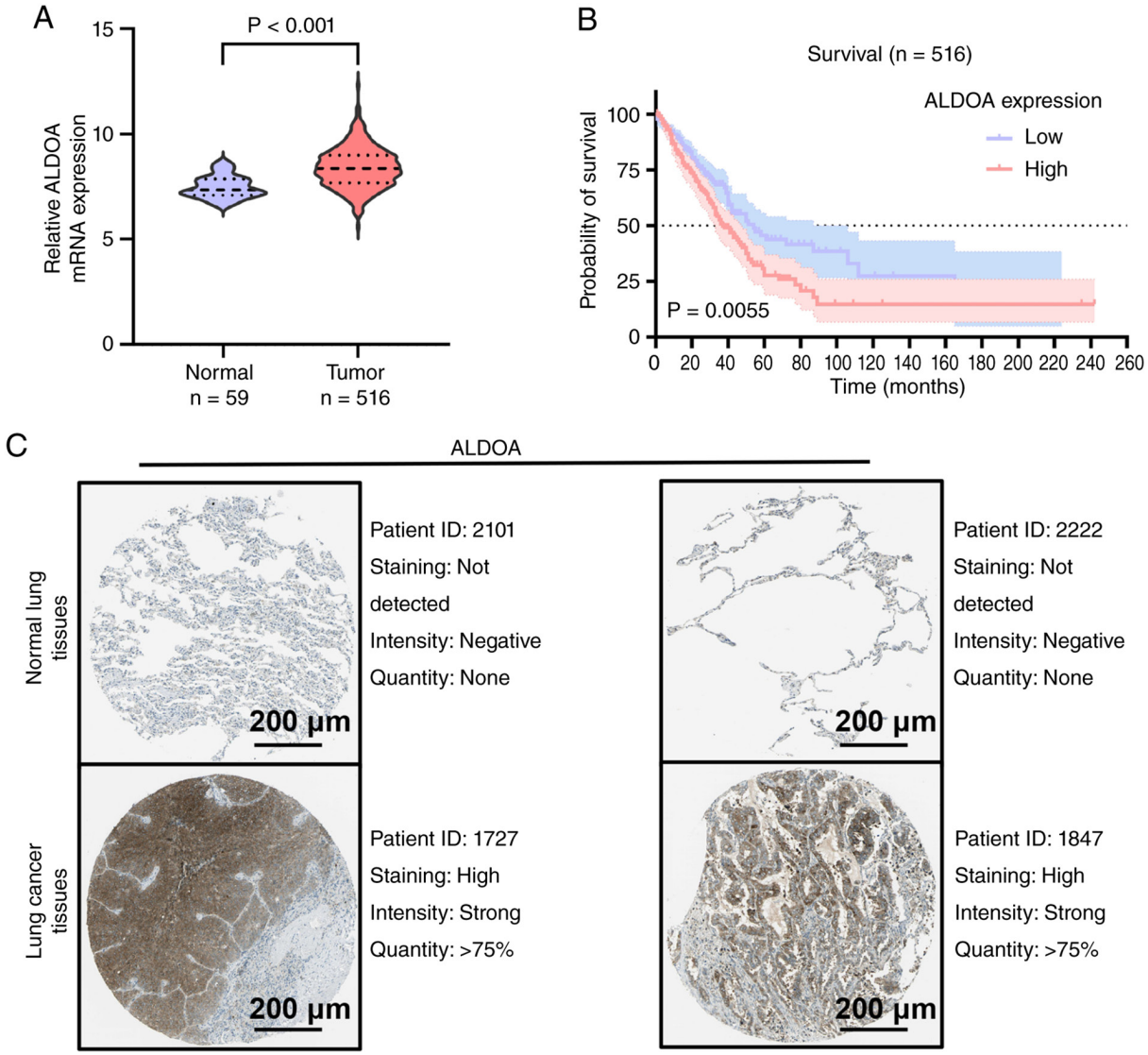


Figure 2. ALDOA is highly expressed in LUAD and predicts poor prognosis. (A) Differential expression analysis of ALDOA in lung cancer tissues (Tumor) and normal lung tissues (Normal) based on The Cancer Genome Atlas database. (B) Kaplan-Meier survival analysis showing overall survival of patients with lung cancer stratified by ALDOA expression levels. (C) Representative immunohistochemical staining images of ALDOA protein expression in normal lung tissues and lung cancer tissues obtained from the Human Protein Atlas database (scale bar, 200 μm). Statistical analysis was performed using an unpaired Student's t-test (A) and the log-rank test (B). ALDOA, aldolase A; LUAD, lung adenocarcinoma.

cells. Collectively, these findings indicate that GAA induced mitochondrial apoptosis in LUAD cells through coordinated regulation of Bcl-2 family proteins and caspase activation.

ALDOA is upregulated in LUAD and is associated with unfavorable overall survival. Given that A549 cells are derived from LUAD, the present study performed clinical-level analyses using LUAD datasets to ensure pathological consistency between *in vitro* experiments and patient-derived data. Transcriptomic data from TCGA were analyzed to characterize ALDOA expression patterns in patients with LUAD. As shown in Fig. 2A, ALDOA expression was significantly elevated in tumor tissues compared with normal lung tissues. Kaplan-Meier survival analysis further demonstrated that patients with high ALDOA expression exhibited significantly worse overall survival than those with low expression, consistent with a previous report (Fig. 2B) (27). These results were further supported at the protein level by immunohistochemical evidence from the HPA, which exhibited higher ALDOA staining in LUAD tissues (Fig. 2C). Collectively, these results indicate that ALDOA was aberrantly upregulated in LUAD and was significantly associated with unfavorable clinical outcomes, supporting the clinical relevance of ALDOA dysregulation in LUAD.

ALDOA upregulation is associated with enhanced glycolytic activity and suppressed apoptosis in LUAD. Differential expression analysis based on the TCGA-LUAD cohort identified a total of 3,766 DEGs, including 2,356 upregulated and 1,410 downregulated genes in tumor tissues compared with normal lung tissues. Notably, ALDOA was significantly upregulated in LUAD samples, exhibiting a notable fold change and strong statistical significance (Fig. 3A). GO enrichment analysis revealed that these DEGs were primarily enriched in biological processes including 'wound healing', 'B cell mediated immunity' and 'immunoglobulin

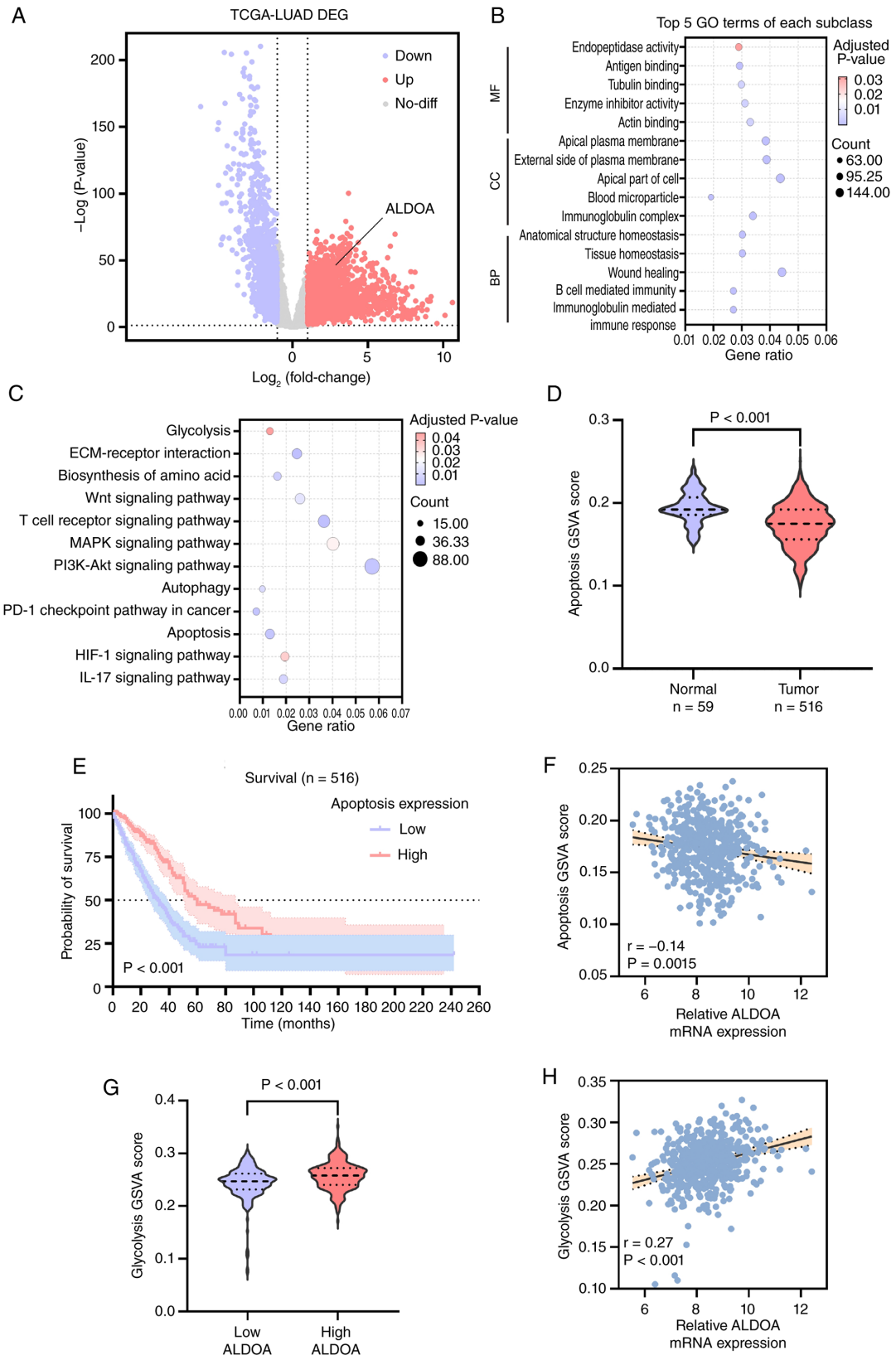


Figure 3. ALDOA overexpression is associated with enhanced glycolytic activity and suppressed apoptosis in LUAD. (A) DEGs between tumor and normal lung tissues in the TCGA cohort. DEGs were defined using an adjusted P<0.05 and $\log_2$ fold change >1, with P-values adjusted using the Benjamini-Hochberg method. (B) GO enrichment analysis of DEGs. (C) KEGG pathway enrichment analysis. For GO and KEGG enrichment analyses, Benjamini-Hochberg-adjusted P<0.05 was considered to indicate a statistically significant difference. (D) Comparison of apoptosis-related gene expression scores between normal and tumor tissues. (E) Kaplan-Meier survival analysis. (F) Correlation analysis. (G) Comparison of KEGG glycolysis/gluconeogenesis GSVA scores between the ALDOA-low and ALDOA-high groups in the TCGA-LUAD cohort. Samples were divided according to the median ALDOA expression level (n=258 per group). (H) Correlation between ALDOA mRNA expression and the KEGG glycolysis/gluconeogenesis GSVA score in LUAD samples. Pearson correlation analysis was performed. Statistical comparisons were performed using an unpaired Student's t-test (D) and a two-sided Mann-Whitney U test (G) Nominal P-values were reported for the prespecified GSVA and correlation analyses. ALDOA, aldolase A; LUAD, lung adenocarcinoma; DEGs, differentially expressed genes; TCGA, The Cancer Genome Atlas; GO, Gene Ontology; KEGG, Kyoto Encyclopedia of Genes and Genomes; GSVA, Gene Set Variation Analysis.

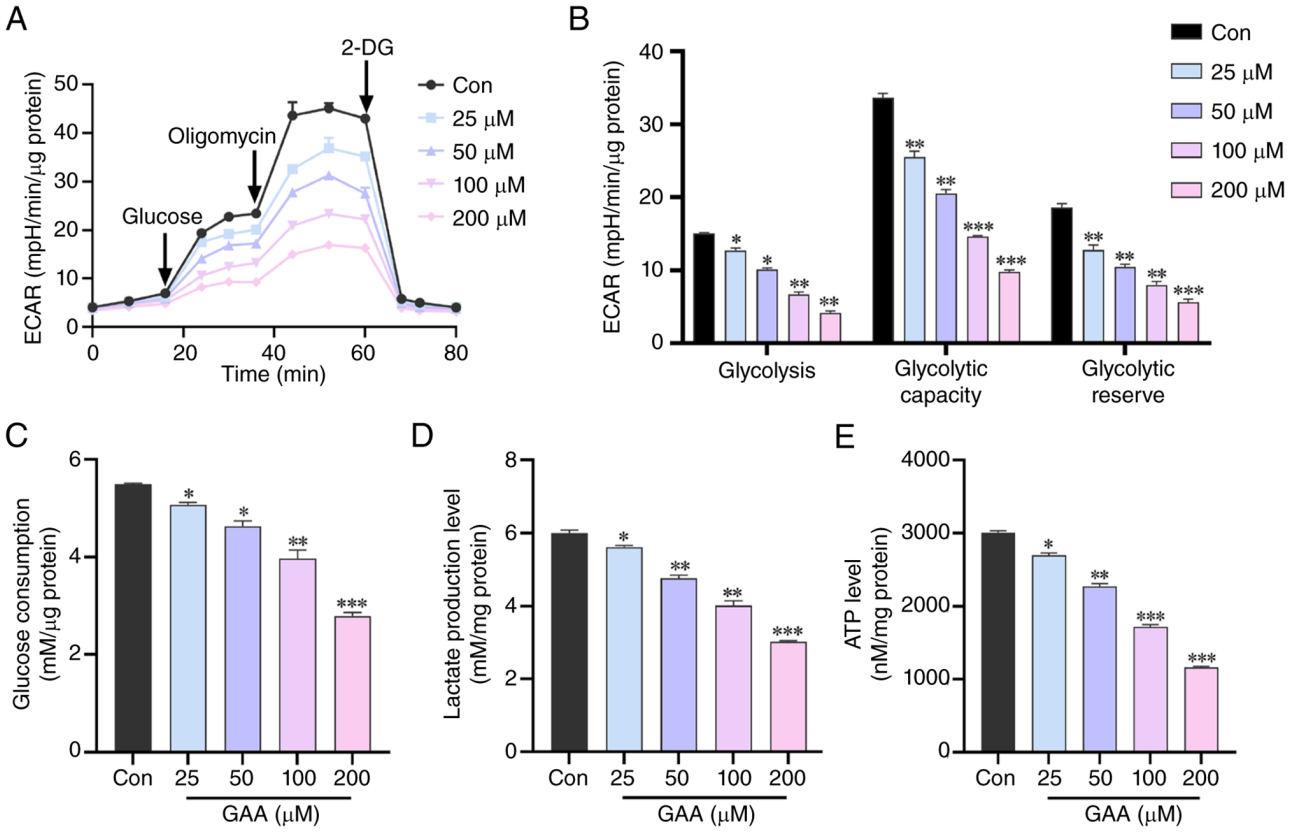


Figure 4. GAA suppresses glycolytic metabolism in A549 cells. (A) ECAR profiles of A549 cells treated with increasing concentrations of GAA (0, 25, 50, 100 and 200 μM). ECAR was monitored during the glycolytic stress assay following sequential addition of glucose, oligomycin and 2-DG. (B) Quantification of glycolysis, glycolytic capacity and glycolytic reserve derived from the ECAR profiles. (C) Glucose consumption in A549 cells following treatment with the indicated concentrations of GAA. (D) Lactate production in A549 cells following GAA treatment. (E) Cellular ATP levels in A549 cells treated with increasing concentrations of GAA. Data are presented as mean ± SEM from three independent experiments. Statistical significance was assessed using one-way ANOVA followed by Bonferroni's multiple-comparison test. *P<0.05, **P<0.01 and ***P<0.001 vs. control. GAA, ganoderic acid A; ECAR, extracellular acidification rate; Con, control; 2-DG, 2-deoxy-D-glucose.

mediated immune response', highlighting marked alterations in the tumor microenvironment and immune regulation during LUAD progression (Fig. 3B). KEGG pathway analysis further demonstrated significant enrichment in canonical oncogenic pathways, including 'PI3K-Akt signaling pathway', 'MAPK signaling pathway', 'ECM-receptor interaction' and 'apoptosis'. In addition, pathways associated with 'PD-1 checkpoint pathway in cancer', 'Autophagy' and 'IL-17 signaling pathway' were significantly represented, underscoring coordinated dysregulation of cell fate determination and immune modulation in LUAD (Fig. 3C).

Importantly, apoptosis-related genes were significantly downregulated in tumor tissues compared with normal controls, indicating that suppression of apoptotic signaling constitutes a key molecular feature of LUAD (Fig. 3D). Kaplan-Meier survival analysis further demonstrated that patients with lower apoptosis signature scores exhibited significantly poorer overall survival (Fig. 3E), supporting the prognostic relevance of apoptosis dysregulation. To clarify the association between ALDOA and apoptotic activity, correlation analysis was performed, revealing a significant negative correlation between ALDOA expression and the apoptosis signature (Fig. 3F).

Given the canonical role of ALDOA as a key glycolytic enzyme, the present study next investigated whether ALDOA expression was associated with glycolytic activity in LUAD. GSVA was performed using the KEGG glycolysis/gluconeogenesis gene set. Based on the median ALDOA expression level, the 516 TCGA-LUAD samples were divided into ALDOA-high and ALDOA-low groups (n=258 per group). The glycolysis GSVA score was significantly higher in the ALDOA-high group compared with the ALDOA-low group (Fig. 3G). Consistently, ALDOA expression exhibited a significant positive correlation with the glycolysis GSVA score across LUAD samples (Fig. 3H). Together with the aforementioned negative association between ALDOA expression and apoptosis activity, these findings indicated that elevated ALDOA expression in LUAD was associated with a metabolic phenotype characterized by enhanced glycolytic activity and reduced apoptotic activity.

GAA suppresses glycolytic metabolism in A549 cells. Given the positive association between ALDOA expression and glycolytic activity observed in the TCGA-LUAD cohort, the present study next investigated whether GAA affects glycolytic metabolism at the functional level in A549 cells. ECAR was first evaluated using a glycolytic stress assay. Following sequential addition of glucose, oligomycin and 2-DG, control A549 cells exhibited the expected increase in ECAR after glucose and oligomycin stimulation, followed by a rapid

decrease after 2-DG administration (Fig. 4A). By contrast, GAA treatment progressively attenuated the ECAR response in a concentration-dependent manner. Quantitative analysis further showed that GAA significantly reduced glycolysis, glycolytic capacity and glycolytic reserve, with progressively greater inhibition observed at increasing concentrations of GAA (Fig. 4B). These findings indicated that GAA suppressed both basal glycolytic activity and the ability of A549 cells to increase glycolytic flux in response to energetic demand.

To further characterize the metabolic consequences of GAA treatment, glucose consumption, lactate production and intracellular ATP levels were measured. GAA treatment resulted in a significant concentration-dependent reduction in glucose consumption (Fig. 4C) and lactate production (Fig. 4D), consistent with suppression of glycolytic metabolism. Cellular ATP levels were also significantly decreased following GAA treatment, with the most notable reduction observed at the highest concentration tested (Fig. 4E). Given that higher concentrations of GAA also caused marked reductions in cell viability, additional experiments were performed to determine whether the metabolic effects remained detectable at substantially lower concentrations. An expanded concentration-response analysis demonstrated a concentration-dependent reduction in A549 cell viability, with a 24-h IC_{50} of 136.5 μM (95% CI: 115.8-162.2 μM; Fig. S1A and B).

Based on this concentration-response relationship, 6.25 and 12.5 μM GAA, both notably below the calculated IC_{50}, were selected for additional metabolic analyses. Under these low-dose conditions, Seahorse glycolytic stress analysis showed that GAA continued to reduce ECAR-derived glycolytic parameters. Both 6.25 and 12.5 μM GAA decreased glycolysis and glycolytic capacity, whereas a significant reduction in glycolytic reserve was observed at 12.5 μM (Fig. S1C). In parallel, OCR was monitored following sequential addition of oligomycin, FCCP and antimycin A. OCR was comparatively less affected, as 6.25 μM GAA produced no significant change in basal OCR or maximum OCR after FCCP, whereas 12.5 μM GAA caused modest but statistically significant reductions in these parameters (Fig. S1D). These findings indicate that the suppression of glycolytic activity at low GAA concentrations cannot be explained solely by the extensive loss of viable cells observed at higher concentrations.

Collectively, these functional metabolic analyses demonstrated that GAA suppressed glycolytic metabolism in A549 cells, as evidenced by reduced ECAR, glycolytic capacity, glucose utilization, lactate production and ATP generation. The persistence of glycolytic inhibition at concentrations markedly below the IC_{50}, together with the comparatively limited changes in OCR, further supports a metabolic effect of GAA beyond the non-specific consequences of extensive cytotoxicity. Collectively, with the positive association between ALDOA expression and glycolytic activity identified in LUAD samples, these findings provide functional metabolic support for a potential association between GAA treatment and ALDOA-associated metabolic regulation.

Network analysis identifies core regulators of apoptosis in LUAD. To further characterize the molecular interaction network underlying apoptosis dysregulation in LUAD, a PPI network was constructed using 87 genes from the apoptosis-related gene set. The genes were imported into the STRING database using a minimum interaction score of 0.9 and disconnected nodes were excluded from visualization. The resulting network comprised 87 nodes and 1,218 edges, revealing extensive interactions among apoptosis-associated proteins (Fig. 5A). To identify highly connected components within this network, the STRING interaction data were subsequently imported into Cytoscape for topological analysis. Degree centrality was calculated for each node and proteins with higher connectivity were visualized as more prominent nodes within the reconstructed network (Fig. 5B). Ranking according to degree centrality identified a number of highly connected apoptosis-related proteins, with *CASP3*, *TNF* and *BCL2* among the top-ranked nodes (Fig. 5C).

Further network topology analysis using the CytoNCA plugin identified *CASP3*, *TNF* and *BCL2* as key hub proteins within the apoptosis-related interaction network (Fig. 5D) (61). Notably, *BCL2* and *CASP3* were also experimentally affected by GAA treatment in A549 cells, as shown by the aforementioned apoptosis-related protein analyses. These findings provide network-level support for the central involvement of *BCL2*- and *CASP3*-associated apoptotic signaling in LUAD and are consistent with the pro-apoptotic phenotype induced by GAA.

ALDOA expression is associated with altered immune infiltration patterns in LUAD. Given the association between tumor metabolic reprogramming and the immune microenvironment and the present finding that elevated ALDOA expression was associated with enhanced glycolytic activity in LUAD, the present study next investigated whether ALDOA expression was also associated with changes in immune cell infiltration. CIBERSORT was applied to TCGA-LUAD transcriptomic data to estimate the relative proportions of 22 immune cell subsets in tumor and normal lung tissues.

As shown in Fig. 6A, LUAD tissues exhibited broad alterations in immune cell composition compared with normal lung tissues. Among adaptive immune cell populations, naïve B cells and plasma cells exhibited significantly increased infiltration in tumor tissues, as did activated memory $CD4^+$ T cells, follicular helper T cells and regulatory T cells. Among innate immune populations, macrophages M0, resting mast cells, monocytes, resting natural killer cells, eosinophils and neutrophils were significantly decreased, whereas macrophages M1 and resting dendritic cells were significantly increased, indicating notable restructuring of the immune landscape in LUAD (62). To further characterize associations among these immune populations, pairwise correlation analysis was performed across the 22 immune cell subsets (Fig. 6B). The resulting correlation matrix revealed coordinated and opposing patterns among multiple immune populations, highlighting the complex organization of the LUAD immune microenvironment.

The present study next examined the association between ALDOA expression and immune cell infiltration. ALDOA expression was notably associated with the abundance of numerous immune cell subsets, including positive correlations with macrophages M0, activated mast cells and neutrophils, and negative correlations with naïve B cells, resting mast cells and resting memory $CD4^+$ T cells (Fig. 6C). Both positive and negative associations were observed across adaptive and

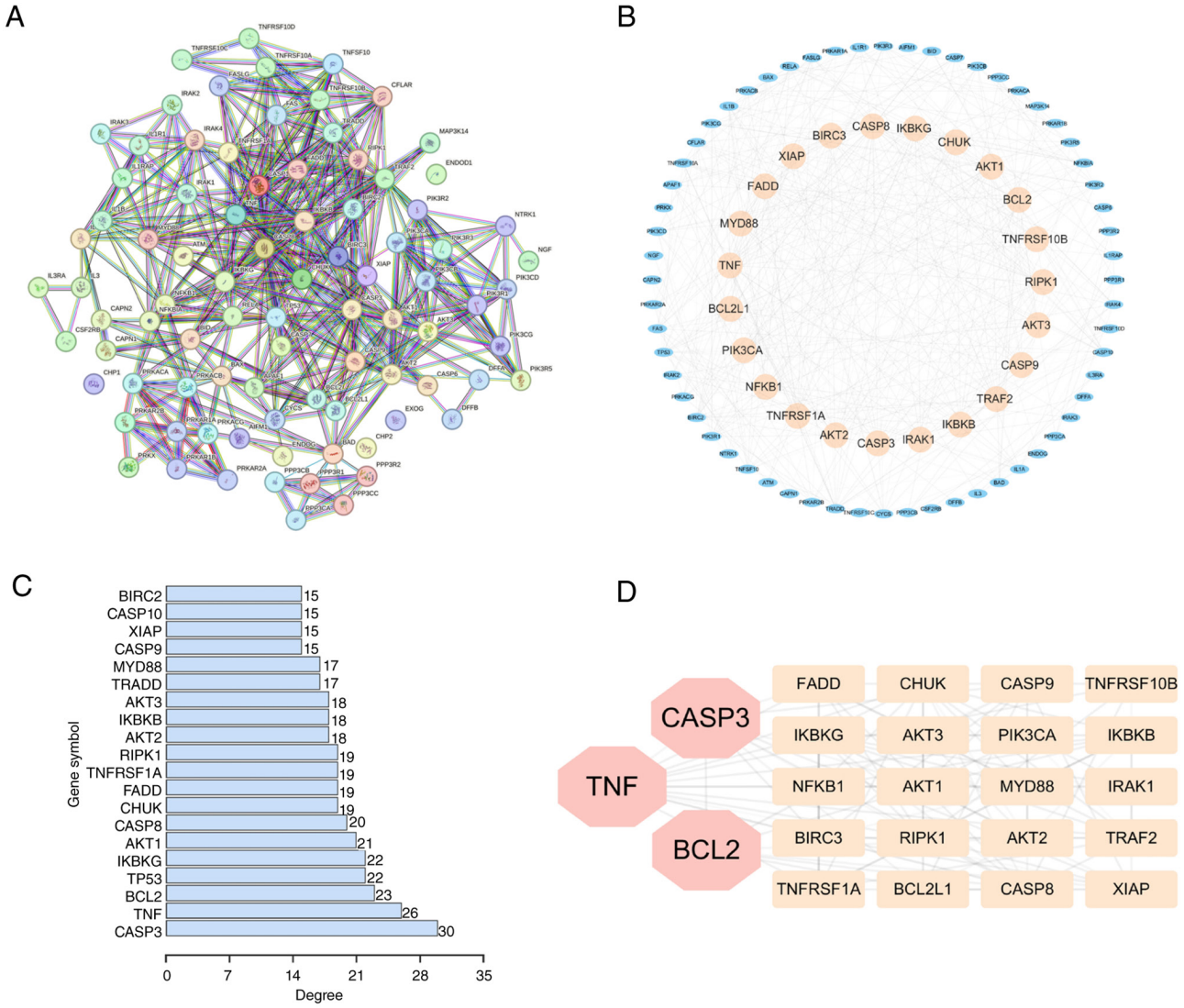


Figure 5. PPI network analysis identifies core apoptosis-related regulators in lung adenocarcinoma. (A) PPI network of apoptosis-related genes. (B) Visualization of the apoptosis-related PPI network based on degree values calculated using Cytoscape. (C) Bar plot showing the top 20 apoptosis-related genes ranked by degree value in the PPI network. (D) Identification of core apoptosis-related hub genes using the CytoNCA plugin. PPI, protein-protein interaction.

innate immune populations, suggesting that ALDOA expression is linked to distinct immune infiltration patterns rather than to a uniform change in overall immune abundance. In Fig. 6C, red and cyan dots indicate negative and positive correlations, respectively and dot size reflects the magnitude of the correlation.

Collectively, these findings indicated that elevated ALDOA expression in LUAD was associated not only with enhanced glycolytic activity and reduced apoptotic activity, but also with an altered immune infiltration profile. These observations extend the clinical relevance of ALDOA from tumor cell metabolism and apoptosis to the immune microenvironment, while the causal association between ALDOA activity and immune remodeling remains to be established experimentally.

WGCNA identifies an ALDOA-containing co-expression module associated with apoptosis in LUAD. To further investigate the molecular network context of ALDOA in LUAD, WGCNA was performed using the TCGA-LUAD transcriptomic dataset. The optimal soft-thresholding power was selected according to the scale-free topology criterion while maintaining adequate network connectivity (Fig. 7A). Hierarchical clustering combined with the dynamic tree cut algorithm subsequently identified a number of gene co-expression modules with distinct expression patterns (Fig. 7B). The topological overlap matrix heatmap further demonstrated clear modular organization and relatively strong intramodular connectivity (Fig. 7C).

Notably, module assignment analysis showed that ALDOA was located within the turquoise module. Given the central focus of the present study on the association between ALDOA and apoptosis, the functional properties of the ALDOA-containing turquoise module were further characterised. Functional enrichment analysis showed that genes within this module were involved in numerous cancer-associated biological processes and signaling pathways, including 'cell-cycle' regulation, 'complement and coagulation cascades', 'neuroactive ligand-receptor interaction' and 'apoptosis' (Fig. 7D).

Notably, apoptosis was significantly represented among the enriched pathways of the ALDOA-containing module.

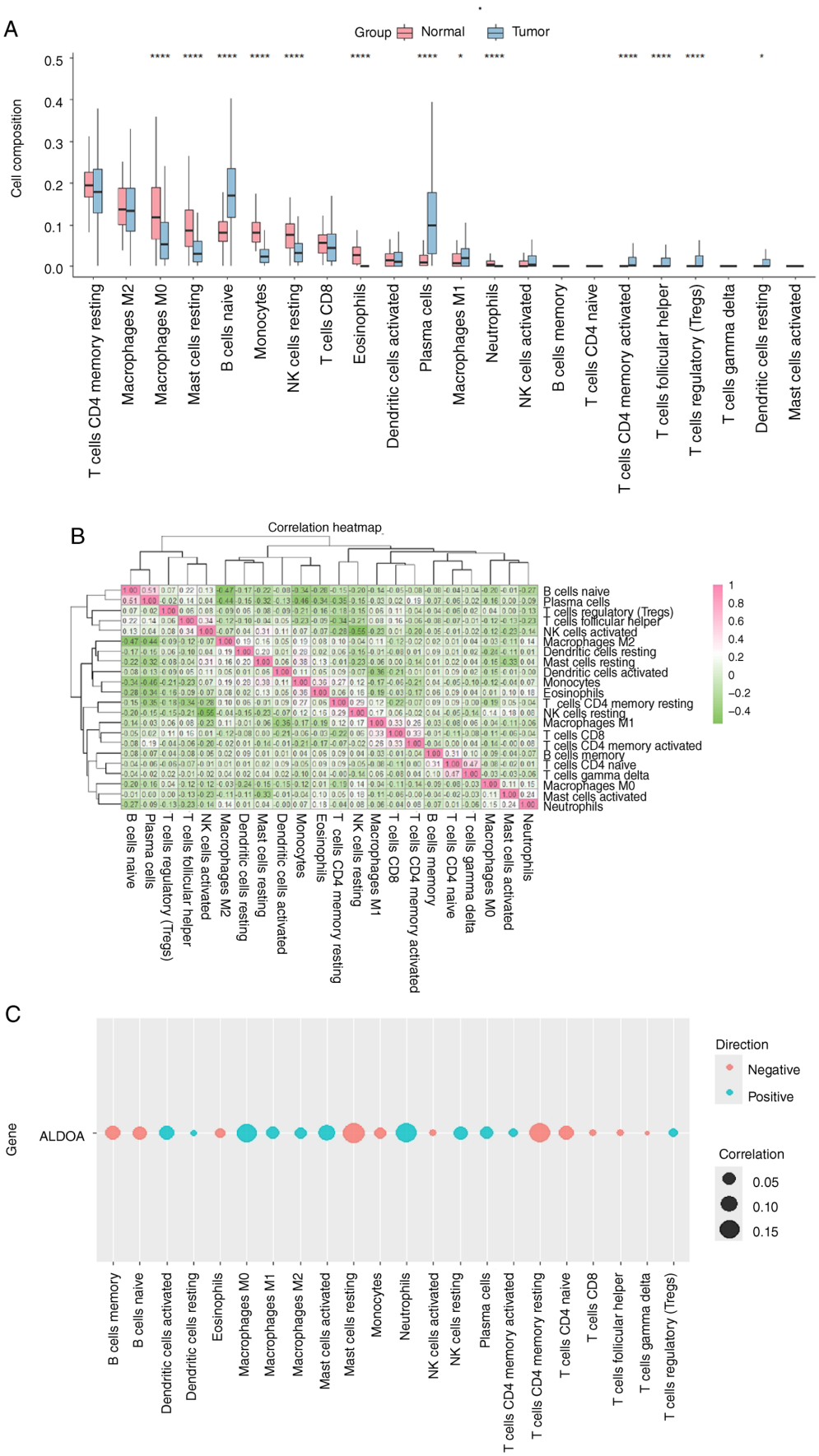


Figure 6. ALDOA expression is associated with altered immune infiltration patterns in LUAD. (A) Comparison of immune cell infiltration between LUAD tissues and normal lung tissues. Differences between tumor and normal tissues were evaluated using the Wilcoxon rank-sum test, with P-values adjusted for multiple comparisons using the Benjamini-Hochberg FDR method. *P<0.05 and ****P<0.0001 vs. normal tissues. (B) Correlation analysis among different immune cell subpopulations. Spearman correlation analysis was performed, with Benjamini-Hochberg FDR correction applied to multiple correlation tests. (C) Correlation between ALDOA expression and immune cell infiltration. ALDOA, aldolase A; LUAD, lung adenocarcinoma; FDR, false discovery rate.

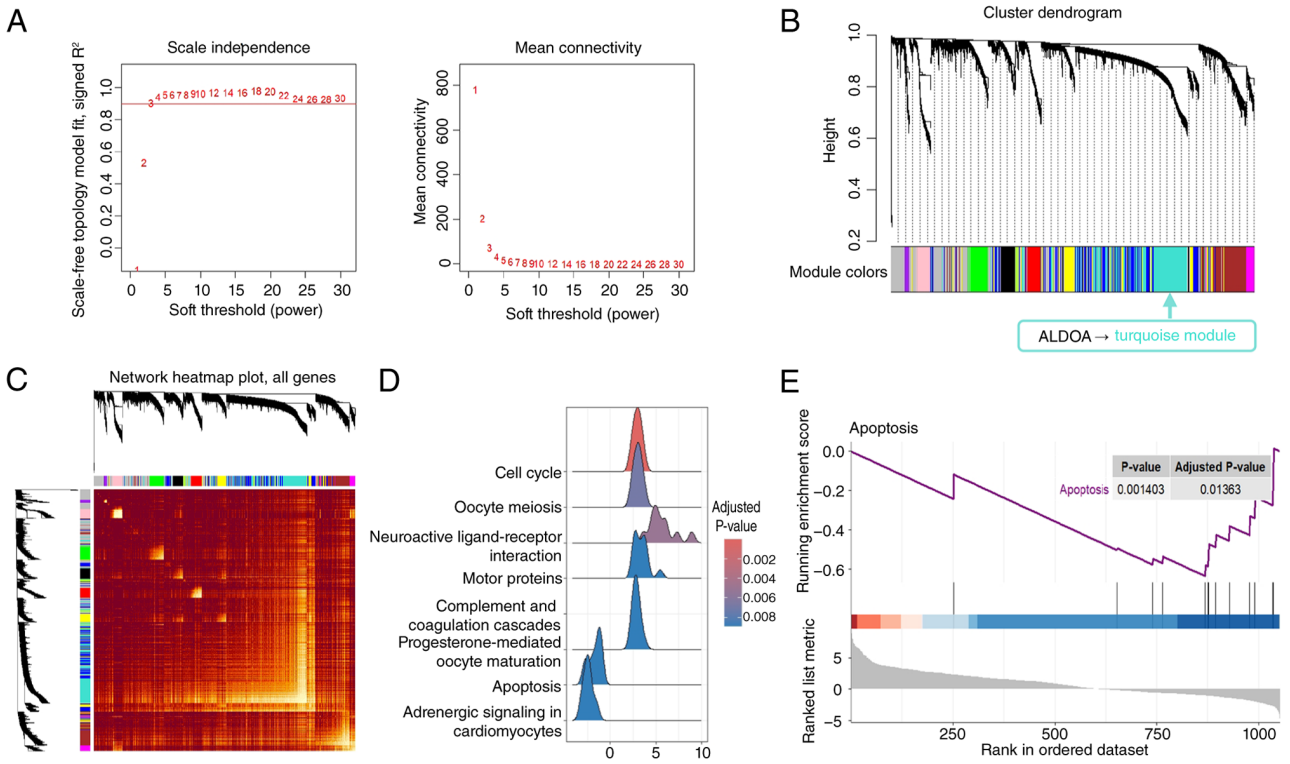


Figure 7. Identification of apoptosis-related gene modules by weighted gene co-expression network analysis. (A) Determination of the optimal soft-thresholding power based on scale-free topology and mean connectivity. (B) Hierarchical clustering dendrogram of genes with module assignments determined using the dynamic tree cut algorithm. ALDOA was assigned to the turquoise module. (C) Network heatmap illustrating the modular structure of the gene co-expression network. (D) Functional enrichment analysis of genes within the ALDOA-containing turquoise module. (E) Gene Set Enrichment Analysis of genes within the ALDOA-containing turquoise module showing significant enrichment of the apoptosis pathway. ALDOA, aldolase A.

GSEA further supported the association of this module with apoptosis-related signaling, with significant enrichment of the apoptosis gene set (Fig. 7E). These findings indicated that ALDOA was embedded within a co-expression module with significant apoptosis-related functional characteristics rather than occurring as an isolated metabolic gene. Collectively, the WGCNA results provide network-level evidence associating ALDOA with apoptosis-associated molecular programs in LUAD and complement the negative association between ALDOA expression and apoptotic activity observed in the preceding GSVA analysis.

Computational and cellular characterization of the putative GAA-ALDOA interaction and GAA-induced suppression of ALDOA expression and aldolase activity. Based on the preceding analyses showing that ALDOA expression was positively associated with glycolytic activity and negatively associated with apoptotic activity in LUAD, together with the functional evidence that GAA suppressed glycolytic metabolism and promoted apoptosis in A549 cells, the present study next investigated whether ALDOA may represent a molecular component associated with the cellular effects of GAA. Molecular docking and molecular dynamics simulations were first performed to characterize the putative interaction between GAA and ALDOA. CETSA was subsequently performed to evaluate GAA-ALDOA target engagement in A549 cells. The present study then examined whether GAA treatment affected ALDOA protein expression and cellular aldolase activity in A549 cells.

Molecular docking predicted that GAA could occupy a pocket within the ALDOA structure and establish multiple non-covalent interactions with surrounding residues (Fig. 8A and B). Hydrogen-bond interactions were predicted with Asp33, Ser35, Lys146 and Asn360, with corresponding interaction distances of 2.341, 1.983, 2.241 and 2.538 Å, respectively. In addition, a salt-bridge interaction was predicted between the carboxyl group of GAA and Arg148. These results suggest a potentially favorable binding configuration between GAA and ALDOA, which was subsequently evaluated using CETSA at the cellular level.

To further evaluate the conformational behavior of the predicted GAA-ALDOA complex, three independent 200-ns MD simulations were conducted. The RMSD trajectories showed an initial equilibration phase followed by relatively stable fluctuations during the remainder of the simulations (Fig. 8C), with mean RMSD values of 0.197±0.028, 0.157±0.014 and 0.196±0.025 nm for the three independent trajectories, respectively. Overall, the RMSD values were largely maintained within ~0.15-0.25 nm, indicating that no marked conformational destabilization occurred during the simulations. Residue-level flexibility was subsequently evaluated by RMSF analysis. Residues surrounding the predicted ligand-binding region, including Asp33, Ser35, Lys146, Arg148 and Asn360, exhibited relatively low fluctuations during the simulations (Fig. 8D), suggesting limited local conformational mobility within the predicted binding region. Consistently, the Rg remained relatively stable throughout the simulations, with an average value of ~1.93±0.02 nm (Fig. 8E), indicating

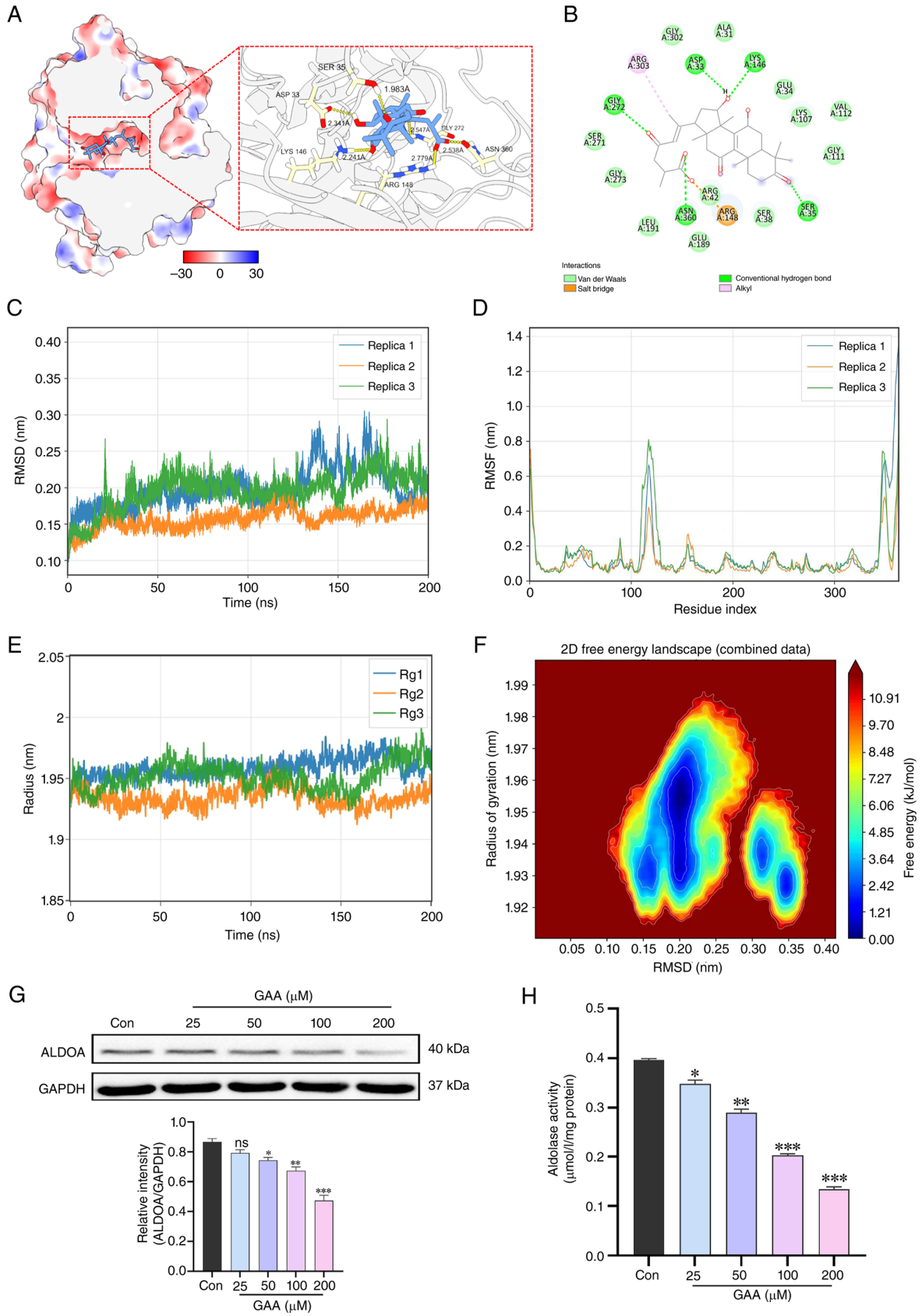


Figure 8. Computational characterization of the putative GAA-ALDOA interaction and the effects of GAA on ALDOA expression and aldolase activity. (A) Predicted binding mode of GAA with ALDOA and enlarged view of the binding pocket. (B) Two-dimensional interaction diagram of the predicted GAA-ALDOA complex. (C) RMSD profiles from three independent 200-ns molecular dynamics simulations. (D) RMSF analysis of ALDOA residues during the simulations. (E) Rg profiles of the GAA-ALDOA complex. (F) Two-dimensional free energy landscape projected onto RMSD and Rg coordinates. (G) Western blotting analysis of ALDOA expression in A549 cells treated with GAA (0, 25, 50, 100 and 200 μM) for 24 h. The relative intensities of proteins were normalized against GAPDH. (H) Cellular aldolase activity following GAA treatment. Data are presented as the mean ± SEM from three independent experiments. Statistical significance was assessed using one-way ANOVA followed by Bonferroni's multiple-comparison test. *P<0.05, **P<0.01 and ***P<0.001 vs. control. ALDOA, aldolase A; GAA, ganoderic acid A; RMSD, root mean square deviation; RMSF, root mean square fluctuation; Rg, radius of gyration.

preservation of the overall compactness of the ALDOA structure.

Free energy landscape analysis using RMSD and Rg as collective variables further revealed two predominant low-energy conformational basins (Fig. 8F). The key low-energy basin was centered at approximately RMSD=0.20 nm and Rg=1.96 nm, whereas a secondary basin was observed at approximately RMSD=0.35 nm and Rg=1.93 nm. These findings indicated that the predicted GAA-ALDOA complex predominantly sampled a limited number of energetically favorable conformational states and further support the conformational stability of the docked complex *in silico*. To experimentally assess cellular target engagement between GAA and ALDOA, CETSA was performed in A549 cells. Compared with the DMSO control, GAA treatment (100 μM) increased the thermal stability of ALDOA, with greater retention of soluble ALDOA protein at elevated temperatures and a rightward shift in the thermal denaturation profile (Fig. S2). Quantitative analysis determined significantly higher relative ALDOA abundance in GAA-treated cells over the higher-temperature range. These findings provide cellular target-engagement evidence supporting a GAA-ALDOA interaction and complement the molecular docking and molecular dynamics results.

The present study further examined the effects of GAA on ALDOA abundance and enzymatic activity. Western blotting analysis showed that GAA progressively reduced ALDOA protein expression in A549 cells in a concentration-dependent manner, with a significant reduction observed at higher concentrations (Fig. 8G). To determine whether this change was accompanied by an alteration in glycolytic enzyme function, cellular aldolase activity was further measured. Consistent with the reduction in ALDOA protein expression, GAA treatment significantly decreased aldolase activity in a concentration-dependent manner (Fig. 8H). These functional changes were concordant with the reductions in ECAR, glucose consumption, lactate production and ATP levels observed following GAA treatment, further indicating an association between GAA exposure and suppression of glycolytic metabolism.

Collectively, the computational analyses predicted a potentially stable interaction between GAA and ALDOA, while CETSA provided additional cellular target-engagement evidence supporting this interaction. The cellular experiments further demonstrated that GAA reduced both ALDOA protein expression and aldolase enzymatic activity in A549 cells. Together with the preceding evidence that ALDOA expression was positively associated with glycolytic activity in LUAD and that GAA suppressed glycolytic metabolism while promoting apoptosis, these findings support an ALDOA-associated metabolic mechanism as a potential contributor to the pharmacological effects of GAA in LUAD cells. Despite this, CETSA did not establish the causal requirement of ALDOA for the metabolic or apoptotic effects of GAA and direct biophysical characterization of GAA-ALDOA binding, the precise binding site and its association with the physiological substrate fructose-1,6-bisphosphate and the molecular mechanism underlying GAA-induced ALDOA downregulation remain to be further established.

Discussion

Advanced lung adenocarcinoma is characterized by notable molecular heterogeneity, aggressive metastatic behavior and frequent resistance to targeted therapies and chemotherapy, all of which contribute to unfavorable clinical outcomes (63,64). Therefore, the identification of pharmacologically active compounds capable of interfering with key tumor survival pathways remains an important therapeutic objective. *G. lucidum* is one of the most extensively studied medicinal fungi in cancer-related research (65). The present study found that GAA, a key triterpenoid derived from *G. lucidum*, inhibited A549 cell viability and promoted apoptosis. Notably, these effects were accompanied by marked suppression of glycolytic metabolism, suggesting that metabolic interference may represent an important component of the antitumor activity of GAA in LUAD.

Traditional Chinese Medicine and its bioactive constituents have received increasing attention as potential sources of compounds with multi-target pharmacological activities (66). Triterpenoids derived from *G. lucidum* have been extensively investigated for their anti-inflammatory, immunomodulatory and antitumor properties (67,68). GAA, one of the key triterpenoids of *G. lucidum*, has previously been reported to induce apoptosis and inhibit tumor growth through mitochondrial and other apoptosis-related pathways (69-71). However, the metabolic mechanisms underlying its antitumor effects remain less well defined. In the present study, GAA significantly reduced extracellular acidification rate-derived glycolytic parameters, glucose consumption, lactate production and intracellular ATP levels in A549 cells. These findings provide functional evidence that GAA suppresses glycolytic metabolism rather than merely altering the expression of metabolism-related genes. Given that higher GAA concentrations were accompanied by marked reductions in cell viability, additional analyses were performed at 6.25 and 12.5 μM, concentrations notably below the calculated IC_{50}. Glycolysis and glycolytic capacity remained significantly reduced under these low-dose conditions, whereas OCR was comparatively less affected. This finding indicates that the suppression of glycolytic metabolism cannot be explained solely by the extensive loss of viable cells at higher concentrations, while also suggesting that the effect of GAA should not be interpreted as exclusively selective for glycolysis. Given the dependence of rapidly proliferating tumor cells on glycolytic energy production, such metabolic suppression may contribute to the reduced viability and enhanced apoptosis observed following GAA treatment.

ALDOA has emerged as a potentially relevant molecular component linking the metabolic and apoptotic effects of GAA. ALDOA is a central glycolytic enzyme responsible for the cleavage of fructose-1,6-bisphosphate and has increasingly been recognized to possess additional functions in tumor progression. Previous studies have shown that ALDOA contributes to proliferation, migration, invasion and chemoresistance in numerous malignancies (72,73). Its upregulation has been reported in numerous solid tumors, including lung, liver and pancreatic cancers and is frequently associated with aggressive tumor behavior and poor prognosis (27,74). Mechanistically, ALDOA has been implicated in the regulation of signaling pathways such as EGFR/MAPK, thereby promoting tumor

cell proliferation and survival (28). Consistent with these observations, the present analysis showed that ALDOA was significantly upregulated in LUAD and that higher ALDOA expression was associated with unfavorable overall survival. HPA data further supported increased ALDOA protein expression in LUAD tissues. However, these findings represent discovery-level evidence and do not establish ALDOA as a clinically validated prognostic or predictive biomarker. Translation of ALDOA toward biomarker application would require confirmation in independent patient cohorts, external validation of its prognostic performance and integration with additional clinical and molecular variables (75).

Accordingly, ALDOA should currently be considered a candidate or potential biomarker rather than an established clinical biomarker. The present pathway-level analyses further demonstrated an association between ALDOA and both altered glycolytic and apoptotic states in LUAD. Apoptosis is key in tissue homeostasis, whereas its suppression is a well-established hallmark of malignant progression (76). The mitochondrial apoptotic pathway is controlled by Bcl-2 family proteins and the caspase cascade, with Bax promoting mitochondrial permeabilization and Bcl-2 exerting an opposing anti-apoptotic effect (77). In the present study, ALDOA expression was negatively associated with apoptosis-related pathway activity, whereas higher ALDOA expression was accompanied by increased glycolysis-related GSVA scores. These findings suggest that elevated ALDOA expression may be associated with a metabolic state favoring glycolysis and reduced apoptotic activity in LUAD. Such an association is biologically plausible given that enhanced glycolytic metabolism can influence mitochondrial function, redox homeostasis and cellular survival signaling (78). Metabolic and redox remodeling may further contribute to malignant phenotypes through alterations in ROS homeostasis, whereas increased glycolytic flux and lactate accumulation can influence tumor progression, treatment response and lactate-associated signaling and epigenetic regulation (79,80). These observations place the GAA-induced reductions in glycolytic activity and lactate production within a broader metabolic context rather than representing an isolated alteration in glucose utilization. Consistently, GAA treatment reduced Bcl-2 expression, increased Bax expression and promoted caspase-3 activation, as evidenced by elevated cleaved caspase-3 levels and altered total caspase-3 expression in A549 cells. These findings indicate that GAA modulates key components of the mitochondrial apoptotic pathway and shifts the cellular balance toward apoptosis. Protein-protein interaction analysis further identified *CASP3*, *BCL2* and *TNF* as central nodes within the apoptosis-related network, supporting the importance of apoptotic regulation in the biological context examined in the present study.

The functional metabolic findings suggest an additional association between ALDOA and the pharmacological effects of GAA. GAA treatment not only suppressed ECAR, glucose consumption, lactate production and ATP generation, but also reduced cellular aldolase activity in a concentration-dependent manner. These results are consistent with the observed reduction in ALDOA protein expression and support the possibility that suppression of an ALDOA-associated glycolytic process contributes to the metabolic effects of GAA. Notably, however, the present data does not establish that ALDOA is the sole mediator of GAA-induced glycolytic inhibition. GAA may affect numerous metabolic proteins and signaling pathways and cellular aldolase activity reflects the overall activity of aldolase enzymes rather than exclusively ALDOA. Therefore, ALDOA should currently be regarded as a mechanistically relevant candidate associated with the metabolic response to GAA rather than as a definitively established molecular mediator.

The WGCNA results provided further systems-level support for the involvement of ALDOA in apoptosis-related regulation. ALDOA was assigned to the turquoise co-expression module and functional characterization of the ALDOA-containing module exhibited enrichment of apoptosis-related signaling. These observations complement the negative association between ALDOA expression and apoptosis-related pathway activity and suggest that ALDOA is embedded within a broader transcriptional network related to tumor cell survival. Rather than indicating a direct regulatory association, the WGCNA findings provide network-level evidence that ALDOA and apoptosis-associated genes may participate in coordinated biological programs in LUAD.

In addition to metabolic and apoptotic alterations, ALDOA expression was associated with changes in the immune infiltration profile of LUAD. Alterations involving $CD8^+$ T cells, regulatory T cells, activated $CD4^+$ T cells and macrophage populations were observed in the transcriptomic analyses. Tumor metabolic reprogramming can influence immune cell function through nutrient competition, lactate accumulation and changes in the local metabolic environment (81). Persistent metabolic and inflammatory signaling may further reshape immune-cell states and contribute to an immunosuppressive or treatment-resistant tumor microenvironment (82-85). Thus, the association between ALDOA expression and altered immune infiltration observed in the present study is biologically consistent with a broader association between tumor metabolic reprogramming and immune regulation. Accordingly, the association between ALDOA expression and altered immune infiltration may reflect a broader relationship between tumor glycolytic activity and the immune microenvironment. Despite this, these findings should be interpreted as associative rather than causal. The present study did not directly examine the effects of GAA on immune cells, nor did it demonstrate that ALDOA regulates immune cell infiltration. Therefore, the immune analysis primarily provides clinical-contextual evidence supporting the broader biological relevance of ALDOA in LUAD rather than establishing an ALDOA-dependent immunomodulatory mechanism of GAA.

Molecular docking and molecular dynamics simulations further suggested that GAA could adopt a potentially stable binding configuration within a predicted pocket of ALDOA. The predicted interaction involved hydrogen bonding and salt bridge formation, while RMSD, RMSF, Rg and free energy landscape analyses indicated that the modeled complex maintained relative conformational stability during the simulations. These computational findings provide structural support for a possible GAA-ALDOA interaction. However, docking and molecular dynamics simulations alone cannot establish direct molecular binding under physiological conditions. Therefore, these results should be interpreted as hypothesis-generating evidence rather than definitive proof that ALDOA is a direct

molecular target of GAA. Consistent with these computational predictions, CETSA demonstrated increased thermal stability of ALDOA following GAA treatment, providing cellular target-engagement evidence supporting a GAA-ALDOA interaction. Despite this, CETSA does not establish direct biophysical binding or demonstrate that ALDOA is causally required for the metabolic and apoptotic effects of GAA. The accompanying reduction in ALDOA protein expression and cellular aldolase activity after GAA treatment further strengthens the functional association between GAA and ALDOA-related metabolism but does not establish the causal requirement of ALDOA for the pharmacological effects of GAA.

A number of limitations within the present study should therefore be acknowledged. First, experimental validation was primarily performed in A549 cells and confirmation in additional LUAD cell lines, animal models and patient-derived systems will be necessary to establish the generalizability and translational relevance of the present findings. In addition, higher concentrations of GAA were associated with notable reductions in cell viability and metabolic alterations observed under these conditions should therefore be interpreted cautiously. Although additional low-dose ECAR and OCR analyses reduced the likelihood that the glycolytic phenotype was solely attributable to extensive cytotoxicity, changes in cell viability may still partly contribute to metabolic alterations at higher GAA concentrations. Second, although the present study demonstrated associations among ALDOA expression, glycolytic activity and apoptosis, the causal contribution of ALDOA to the pharmacological effects of GAA remains to be established. Genetic gain and loss of function experiments, particularly ALDOA overexpression rescue studies, will be important to determine whether restoration of ALDOA can reverse GAA-induced glycolytic suppression and apoptosis. Third, CETSA showed that GAA increased the thermal stability of ALDOA in A549 cells, providing cellular target-engagement evidence that supports a GAA-ALDOA interaction. However, CETSA does not establish direct biophysical binding or demonstrate that ALDOA is causally required for the metabolic and apoptotic effects of GAA. Further validation using approaches such as MST or SPR, together with enzyme kinetic and genetic rescue studies, will be required to define the binding characteristics, functional consequences and causal relevance of the GAA-ALDOA interaction. Finally, although ALDOA expression was associated with immune infiltration patterns, the causal relationship between ALDOA-associated metabolic changes and immune remodeling requires validation in appropriate *in vivo* models.

Collectively, the present findings indicate that GAA suppresses glycolytic metabolism and promotes apoptosis in A549 LUAD cells. Integrated functional, transcriptomic, network, cellular target-engagement and computational analyses further identify ALDOA as a potentially relevant metabolic component associated with these pharmacological effects. The CETSA results strengthen the experimental evidence supporting a cellular interaction between GAA and ALDOA, while the absence of genetic rescue and direct biophysical binding data limits assignment of ALDOA as a definitive molecular target or causal mediator of GAA. Accordingly, the present evidence supports a model in which ALDOA-associated glycolytic regulation may contribute to the antitumor effects of GAA. These findings provide a mechanistic basis for further investigation of GAA as a metabolic modulator in LUAD and highlight ALDOA-associated glycolytic regulation as a potential pharmacological vulnerability.

In conclusion, GAA suppresses glycolytic metabolism and promotes apoptosis in A549 LUAD cells. Integrated experimental, transcriptomic, network, cellular target-engagement and computational analyses further identify ALDOA as a potentially relevant metabolic component associated with these effects. GAA reduced ALDOA protein expression and cellular aldolase activity, while CETSA provided cellular evidence supporting GAA-ALDOA target engagement, complemented by molecular docking and molecular dynamics simulations. These findings suggest that modulation of ALDOA-associated glycolytic regulation may contribute to the antitumor activity of GAA and provide a basis for further mechanistic validation in LUAD.

Acknowledgements

Not applicable.

Funding

No funding was received.

Availability of data and materials

The data generated in the present study may be requested from the corresponding author.

Authors' contributions

LM and YC contributed equally to the present study. LM and YC performed the experiments, collected the data, analyzed the data, prepared the figures and wrote the original draft of the manuscript. QZ, YT and SD assisted with data collection. HL and JX conceived and designed the present study, interpreted the data, supervised the project, revised the manuscript and are the corresponding authors. LM and YC confirm the authenticity of all the raw data. All authors read and approved the final version of the manuscript.

Ethics approval and consent to participate

Not applicable.

Patient consent for publication

Not applicable.

Competing interests

The authors declare that they have no competing interests.

References

1. Bray F, Laversanne M, Sung H, Ferlay J, Siegel RL, Soerjomataram I and Jemal A: Global cancer statistics 2022: GLOBOCAN estimates of incidence and mortality worldwide for 36 cancers in 185 countries. CA Cancer J Clin 74: 229-263, 2024.

2. Thai AA, Solomon BJ, Sequist LV, Gainor JF and Heist RS: Lung cancer. Lancet 398: 535-554, 2021.
3. Siegel RL, Giaquinto AN and Jemal A: Cancer statistics, 2024 CA. Cancer J Clin 74: 12-49, 2024.
4. Sung H, Ferlay J, Siegel RL, Laversanne M, Soerjomataram I, Jemal A and Bray F: Global cancer statistics 2020: GLOBOCAN estimates of incidence and mortality worldwide for 36 cancers in 185 countries. CA. Cancer J Clin 71: 209-249, 2021.
5. He S, Xia C, Li H, Cao M, Yang F, Yan X, Zhang S, Teng Y, Li Q and Chen W: Cancer profiles in China and comparisons with the USA: A comprehensive analysis in the incidence, mortality, survival, staging, and attribution to risk factors. Sci China Life Sci 67: 122-131, 2024.
6. Qiu H, Cao S and Xu R: Cancer incidence, mortality, and burden in China: A time-trend analysis and comparison with the United States and United Kingdom based on the global epidemiological data released in 2020. Cancer Commun (Lond) 41: 1037-1048, 2021.
7. Skoulidis F and Heymach JV: Co-occurring genomic alterations in non-small-cell lung cancer biology and therapy. Nat Rev Cancer 19: 495-509, 2019.
8. Walser T, Cui X, Yanagawa J, Lee JM, Heinrich E, Lee G, Sharma S and Dubinett SM: Smoking and lung cancer: The role of inflammation. Proc Am Thorac Soc 5: 811-815, 2008.
9. Riudavets M, Garcia de Herreros M, Besse B and Mezquita L: Radon and lung cancer: Current trends and future perspectives. Cancers (Basel) 14: 3142, 2022.
10. Loomis D, Huang H and Chen G: The international agency for research on cancer (IARC) evaluation of the carcinogenicity of outdoor air pollution: Focus on China. Chin J Cancer 33: 189-196, 2014.
11. US Preventive Services Task Force; Krist AH, Davidson KW, Mangione CM, Barry MJ, Cabana M, Caughey AB, Davis EM, Donahue KE, Doubeni CA, *et al*: Screening for lung cancer: US preventive services task force recommendation statement. JAMA 325: 962-970, 2021.
12. Wang H, Niu X, Jin Z, Zhang S, Fan R, Xiao H and Hu SS: Immunotherapy resistance in non-small cell lung cancer: From mechanisms to therapeutic opportunities. J Exp Clin Cancer Res 44: 250, 2025.
13. Bigler D, Gulding KM, Dann R, Sheabar FZ, Conaway MR and Theodorescu D: Gene profiling and promoter reporter assays: Novel tools for comparing the biological effects of botanical extracts on human prostate cancer cells and understanding their mechanisms of action. Oncogene 22: 1261-1272, 2003.
14. Lu J, Zhang T, Jiang C, Hu H, Fei Y, Yang Y, An H, Qin H, Zhu Z, Yang Y, *et al*: Ganoderic acid a regulates CSF1R to reprogram tumor-associated macrophages for immune therapy of hepatocellular carcinoma. Int Immunopharmacol 161: 114989, 2025.
15. Zhao R, Zhang C, Tang C, Wu X, Hu S, Luo Q, Jia N, Fan L, Wang Y, Jiang W and Chen Q: Triterpenes from ganoderma lucidum inhibit hepatocellular carcinoma by regulating enhancer-associated lncRNA in vivo. J Ethnopharmacol 336: 118706, 2025.
16. Sui Q, Zhu C, Shi S, Xu J, Zhang J, Wang A, Chen P, Liang G and Zhang Y: Ganoderic acid a: An in-depth review of pharmacological effects and molecular docking analysis. J Ethnopharmacol 349: 119868, 2025.
17. Chaudhary UB, Rashid M and Keane TE: PC-SPES withdrawal response. Acta Oncol 43: 772-773, 2004.
18. Cordell GA: PC-SPES: A brief overview. Integr. Cancer Ther 1: 271-286, 2002.
19. Gill BS, Navgeet and Kumar S: Ganoderma lucidum targeting lung cancer signaling: A review. Tumor Biol 39: 1010428317707437, 2017.
20. Liu Y, Ren S, Sang Q, Cheng X and Bi Y: Potential active compounds of ganoderma lucidum and their anticancer effects: A comprehensive review. Food Sci Nutr 13: e70741, 2025.
21. Wu P, Zhang C, Yin Y, Zhang X, Li Q, Yuan L, Sun Y, Zhou S, Ying S and Wu J: Bioactivities and industrial standardization status of ganoderma lucidum: A comprehensive review. Heliyon 10: e36987, 2024.
22. Radwan FF, Perez JM and Haque A: Apoptotic and immune restoration effects of ganoderic acids define a new prospective for complementary treatment of cancer. J Clin Cell Immunol S3: 4, 2011.
23. Cao Y, Xu X, Liu S, Huang L and Gu J: Ganoderma: A cancer immunotherapy review. Front Pharmacol 9: 1217, 2018.
24. Gong E, Pan J, Ye Z, Cai X, Zheng H, Yin Z, Jiang Y, Wang X and Cao Z: Ganoderic acid a suppresses autophagy by regulating the circFLNA/miR-486-3p/CYP1A1/XRCC1 axis to strengthen the sensitivity of lung cancer cells to cisplatin. J Pharm Pharmacol 76: 354-367, 2024.
25. Bashir MA, Abdalla M, Shao CS, Wang H, Bondzie-Quaye P, Almahi WA, Swallah MS and Huang Q: Dual inhibitory potential of ganoderic acid a on GLUT1/3: Computational and in vitro insights into targeting glucose metabolism in human lung cancer. RSC Adv 14: 28569-28584, 2024.
26. Zheng S, Ma J, Zhao X, Yu X and Ma Y: Ganoderic acid a attenuates IL-1β-induced inflammation in human nucleus pulposus cells through inhibiting the NF-κB pathway. Inflammation 45: 851-862, 2022.
27. Lu G, Shi W and Zhang Y: Prognostic implications and immune infiltration analysis of ALDOA in lung adenocarcinoma. Front Genet 12: 721021, 2021.
28. Fu H, Gao H, Qi X, Zhao L, Wu D, Bai Y, Li H, Liu X, Hu J and Shao S: Aldolase a promotes proliferation and G_1/S transition via the EGFR/MAPK pathway in non-small cell lung cancer. Cancer Commun (Lond) 38: 18, 2018.
29. Chang YC, Chan YC, Chang WM, Lin YF, Yang CJ, Su CY, Huang MS, Wu ATH and Hsiao M: Feedback regulation of ALDOA activates the HIF-1α/MMP9 axis to promote lung cancer progression. Cancer Lett 403: 28-36, 2017.
30. Zhou H, Xiao J, Cheng Q, Wang W, Peng H, Lin X, Chen J and Wang X: Metformin inhibits migration and epithelial-to-mesenchymal transition in non-small cell lung cancer cells through AMPK-mediated GDF15 induction. Eur J Pharmacol 985: 177127, 2024.
31. Landi MT, Dracheva T, Rotunno M, Figueroa JD, Liu H, Dasgupta A, Mann FE, Fukuoka J, Hames M, Bergen AW, *et al*: Gene expression signature of cigarette smoking and its role in lung adenocarcinoma development and survival. PLoS One 3: e1651, 2008.
32. Robinson MD, McCarthy DJ and Smyth GK: edgeR: A Bioconductor package for differential expression analysis of digital gene expression data. Bioinformatics 26: 139-140, 2010.
33. Robinson MD and Oshlack A: A scaling normalization method for differential expression analysis of RNA-seq data. Genome Biol 11: R25, 2010.
34. McCarthy DJ, Chen Y and Smyth GK: Differential expression analysis of multifactor RNA-Seq experiments with respect to biological variation. Nucleic Acids Res 40: 4288-4297, 2012.
35. Wickham H: ggplot2: Elegant Graphics for Data Analysis. 2nd Edition. Springer, Cham, 2016. https://doi.org/10.1007/978-3-319-24277-4.
36. Kolde R: pheatmap: Pretty Heatmaps, R package version 1.0.13, 2025. https://doi.org/10.32614/CRAN.package.pheatmap.
37. Kaplan EL and Meier P: Nonparametric estimation from incomplete observations. Journal of the American Statistical Association 53: 457-481, 1958.
38. Wu T, Hu E, Xu S, Chen M, Guo P, Dai Z, Feng T, Zhou L, Tang W, Zhan L, *et al*: clusterProfiler 4.0: A universal enrichment tool for interpreting omics data. Innovation (Camb) 2: 100141, 2021.
39. Yu G: enrichplot: Visualization of Functional Enrichment Result. R package version 1.24.4, Bioconductor, 2024. https://doi.org/10.18129/B9.bioc.enrichplot.
40. Hänzelmann S, Castelo R and Guinney J: GSVA: Gene set variation analysis for microarray and RNA-seq data. BMC Bioinformatics 14: 7, 2013.
41. Liberzon A, Subramanian A, Pinchback R, Thorvaldsdóttir H, Tamayo P and Mesirov JP: Molecular signatures database (MSigDB) 3.0. Bioinformatics 27: 1739-1740, 2011.
42. Cai D, Wang J, Gao B, Li J, Wu F, Zou JX, Xu J, Jiang Y, Zou H, Huang Z, *et al*: RORγ is a targetable master regulator of cholesterol biosynthesis in a cancer subtype. Nat. Commun 10: 4621, 2019.
43. Szklarczyk D, Kirsch R, Koutrouli M, Nastou K, Mehryary F, Hachilif R, Gable AL, Fang T, Doncheva NT, Pyysalo S, *et al*: The STRING database in 2023: Protein-protein association networks and functional enrichment analyses for any sequenced genome of interest. Nucleic Acids Res 51(D1): D638-D646, 2023.
44. Shannon P, Markiel A, Ozier O, Baliga NS, Wang JT, Ramage D, Amin N, Schwikowski B and Ideker T: Cytoscape: A software environment for integrated models of biomolecular interaction networks. Genome Res 13: 2498-2504, 2003.
45. Tang Y, Li M, Wang J, Pan Y and Wu FX: CytoNCA: A Cytoscape plugin for centrality analysis and evaluation of protein interaction networks. Biosystems 127: 67-72, 2015.
46. Pelletier M, Billingham LK, Ramaswamy M and Siegel RM: Extracellular flux analysis to monitor glycolytic rates and mitochondrial oxygen consumption. Methods Enzymol. 542: 125-149, 2014.

47. Cho EJ, Devkota AK, Stancu G, Edupunganti R, Debevec G, Giulianotti M, Houghten R, Powis G and Dalby KN: A robust and cost-effective luminescent-based high-throughput assay for fructose-1,6-bisphosphate aldolase A. SLAS Discov 25: 1038-1046, 2020.
48. Langfelder P and Horvath S: WGCNA: An R package for weighted correlation network analysis. BMC Bioinformatics 9: 559, 2008.
49. Zhang B and Horvath S: A general framework for weighted gene co-expression network analysis. Stat Appl Genet Mol Biol 4: Article 17, 2005.
50. Langfelder P, Zhang B and Horvath S: Defining clusters from a hierarchical cluster tree: The dynamic tree cut package for R. Bioinformatics 24: 719-720, 2008.
51. Newman AM, Liu CL, Green MR, Gentles AJ, Feng W, Xu Y, Hoang CD, Diehn M and Alizadeh AA: Robust enumeration of cell subsets from tissue expression profiles. Nat Methods 12: 453-457, 2015.
52. Newman AM, Steen CB, Liu CL, Gentles AJ, Chaudhuri AA, Scherer F, Khodadoust MS, Esfahani MS, Luca BA, Steiner D, *et al*: Determining cell type abundance and expression from bulk tissues with digital cytometry. Nat Biotechnol 37: 773-782, 2019.
53. Berman HM, Westbrook J, Feng Z, Gilliland G, Bhat TN, Weissig H, Shindyalov IN and Bourne PE: The protein data bank. Nucleic Acids Res 28: 235-242, 2000.
54. Morris GM, Huey R, Lindstrom W, Sanner MF, Belew RK, Goodsell DS and Olson AJ: AutoDock4 and AutoDockTools4: Automated docking with selective receptor flexibility. J Comput Chem 30: 2785-2791, 2009.
55. Sanner MF: A component-based software environment for visualizing large macromolecular assemblies. Structure 13: 447-462, 2005.
56. Eberhardt J, Santos-Martins D, Tillack AF and Forli S: AutoDock vina 1.2.0: New docking methods, expanded force field, and python bindings. J Chem Inf Model 61: 3891-3898, 2021.
57. Trott O and Olson AJ: AutoDock vina: Improving the speed and accuracy of docking with a new scoring function, efficient optimization, and multithreading. J Comput Chem 31: 455-461, 2010.
58. Taylor RC, Cullen SP and Martin SJ: Apoptosis: Controlled demolition at the cellular level. Nat Rev Mol Cell Biol 9: 231-241, 2008.
59. Tait SW and Green DR: Mitochondria and cell death: Outer membrane permeabilization and beyond. Nat Rev Mol Cell Biol 11: 621-632, 2010.
60. Guo D, Guo C, Fang L, Sang T, Wang Y, Wu K, Guo C, Wang Y, Pan H, Chen R and Wang X: Qizhen capsule inhibits colorectal cancer by inducing NAG-1/GDF15 expression that mediated via MAPK/ERK activation. J Ethnopharmacol 273: 113964, 2021.
61. Liu M, Wang Y, Deng W, Xie J, He Y, Wang L, Zhang J and Cui M: Combining network pharmacology, machine learning, molecular docking and molecular dynamic to explore the mechanism of Chufeng Qingpi decoction in treating schistosomiasis. Front Cell Infect Microbiol 14: 1453529, 2024.
62. Liu G, Zhou C, Xiao X, Hu S, Xie B, Wu Z and Xiao J: Unraveling the immunomodulatory mechanisms of quan-du-zhong capsule in diabetic kidney disease via integrated network pharmacology and experimental validation. Endocr Metab Immune Disord Drug Targets 26: e18715303398054, 2026.
63. Siegel RL, Miller KD, Wagle NS and Jemal A: Cancer statistics. 2023. CA Cancer J Clin 73: 17-48, 2023.
64. Herbst RS, Morgensztern D and Boshoff C: The biology and management of non-small cell lung cancer. Nature 553: 446-454, 2018.
65. Wu K, Na K, Chen D, Wang Y, Pan H and Wang X: Effects of non-steroidal anti-inflammatory drug-activated gene-1 on ganoderma lucidum polysaccharides-induced apoptosis of human prostate cancer PC-3 cells. Int J Oncol 53: 2356-2368, 2018.
66. Liu H, Ge Y and Dong Z: Modernization of traditional Chinese medicine in cancer therapy: '3 D' innovative chinese medicine. Chin J Nat Med 24: 189-202, 2026.
67. Paterson RR: Ganoderma-a therapeutic fungal biofactory. Phytochemistry 67: 1985-2001, 2006.
68. Boh B, Berovic M, Zhang J and Zhi-Bin L: Ganoderma lucidum and its pharmaceutically active compounds. Biotechnol Annu Rev 13: 265-301, 2007.
69. Wang X, Sun D, Tai J and Wang L: Ganoderic acid A inhibits proliferation and invasion, and promotes apoptosis in human hepatocellular carcinoma cells. Mol Med Rep 16: 3894-3900, 2017.
70. Yao X, Li G, Xu H and Lü C: Inhibition of the JAK-STAT3 signaling pathway by ganoderic acid A enhances chemosensitivity of HepG2 cells to cisplatin. Planta Med 78: 1740-1748, 2012.
71. Shao J, Li Z, Jiao G, Sun G and Zhou Z: Ganoderic acid A suppresses proliferation and invasion and induces apoptosis in human osteosarcoma cells. Nan Fang Yi Ke Da Xue Xue Bao 35: 619-624, 2015 (In Chinese).
72. Kawai K, Uemura M, Munakata K, Takahashi H, Haraguchi N, Nishimura J, Hata T, Matsuda C, Ikenaga M, Murata K, *et al*: Fructose-bisphosphate aldolase A is a key regulator of hypoxic adaptation in colorectal cancer cells and involved in treatment resistance and poor prognosis. Int J Oncol 50: 525-534, 2017.
73. Lin J, Xia L, Oyang L, Liang J, Tan S, Wu N, Yi P, Pan Q, Rao S, Han Y, *et al*: The POU2F1-ALDOA axis promotes the proliferation and chemoresistance of colon cancer cells by enhancing glycolysis and the pentose phosphate pathway activity. Oncogene 41: 1024-1039, 2022.
74. Yu S, Xue Y, Chen Y, Cao Y, Yang Y, Ge X and Cai X: The multifaceted roles of aldolase A in cancer: Glycolysis, cytoskeleton, translation and beyond. Hum Cell 38: 45, 2025.
75. Yang Z and Chen S: Histone H3K18 lactylation and cisplatin resistance in bladder cancer: Insights from single-cell transcriptomic analysis. J Transl Genet Genom 9: 257-260, 2025.
76. Hanahan D and Weinberg RA: Hallmarks of cancer: The next generation. Cell 144: 646-674, 2011.
77. Youle RJ and Strasser A: The BCL-2 protein family: Opposing activities that mediate cell death. Nat Rev Mol Cell Biol 9: 47-59, 2008.
78. Vander Heiden MG, Cantley LC and Thompson CB: Understanding the warburg effect: The metabolic requirements of cell proliferation. Science 324: 1029-1033, 2009.
79. Wang W, Liu J, Yang H, Wang Z, Xie M, Chen C, Zhou L, Li X and Zhao M: ACOT9, a mitochondrial metabolism-related gene, promotes ROS-associated epithelial remodeling in laryngeal squamous cell carcinoma. J Transl Med 24: 917, 2026.
80. Karri V and Dalia SM: Persistent IFN-γ signaling in acquired resistance to PD-(L)1 blockade in NSCLC. J Transl Genet Genom 9: 352-358, 2025.
81. Chang CH, Qiu J, O'Sullivan D, Buck MD, Noguchi T, Curtis JD, Chen Q, Gindin M, Gubin MM, van der Windt GJ, *et al*: Metabolic competition in the tumor microenvironment is a driver of cancer progression. Cell 162: 1229-1241, 2015.
82. Zhang M, Zhang F, Wang J, Liang Q, Zhou W and Liu J: Comprehensive characterization of stemness-related lncRNAs in triple-negative breast cancer identified a novel prognostic signature related to treatment outcomes, immune landscape analysis and therapeutic guidance: A silico analysis with in vivo experiments. J Transl Med 22: 423, 2024.
83. Wang Y, Wang J, Zeng T and Qi J: Data-mining-based biomarker evaluation and experimental validation of SHTN1 for bladder cancer. Cancer Genet 288-289: 43-53, 2024.
84. Ubaid S, Kushwaha R, Kashif M and Singh V: Comprehensive analysis of oncogenic determinants across tumor types via multi-omics integration. Cancer Genet 298-299: 44-62, 2025.
85. Liu J, Yang H, Wang Z, Ahmad S, Zhou S, Zhou L, Lou D, Guo Z, Li H and Li X: Benchmarking inflammation-nutrition and TyG-related indices for 5-year mortality risk in adults with questionnaire-defined obstructive sleep apnea: A survey-weighted NHANES derivation cohort with multicenter external validation. J Transl Med 24: 901, 2026.

Copyright © 2026 Mu et al. This work is licensed under a Creative Commons Attribution-NonCommercial-NoDerivatives 4.0 International (CC BY-NC-ND 4.0) License.